Distributed Propulsion Aircraft with Aeroelastic Wing Shaping Control for Improved Aerodynamic Efficiency

Nhan T. Nguyen [1]

NASA Ames Research Center, Moffett Field, CA 94035

Kevin Reynolds [2]

NASA Ames Research Center, Moffett Field, CA 94035

Eric Ting [3]

NASA Ames Research Center, Moffett Field, CA 94035

Natalia Nguyen [4]

Universities Space Research Association, Moffett Field, CA 94035

Abstract

This study presents an aeroelastic wing shaping control concept for distributed propulsion aircraft. By leveraging wing flexibility, wing-mounted distributed propulsion can be used to re-twist wing shapes in-flight to improve aerodynamic efficiency. A multidisciplinary approach is used to develop an aero-propulsive-elastic model of a highly flexible wing distributed propulsion transport aircraft. The conceptual model is used to evaluate the aerodynamic benefit of the distributed propulsion aircraft. The initial conceptual analysis shows that an improvement in the aerodynamic efficiency quantity of lift-to-drag ratio L/D is possible with the proposed aeroelastic wing shaping control for distributed propulsion aircraft. Two concepts are studied: single-generator configuration and dual-generator configuration with four propulsors per wing. The baseline aircraft model is NASA Generic Transport Model. A fan performance analysis is developed for propulsion sizing. Cruise performance analysis is conducted to evaluate the potential improvement in the cruise range for the configurations under study. A flutter analysis is performed to address the potential flutter issue as the propulsors are placed toward the wing tip which would cause a reduction in the wing natural frequencies. Flight control considerations are addressed in the context of the engine-out requirement, yaw and roll controls, and yaw damping augmentation using differential thrust.

1 Introduction

Hybrid electric and all-electric propulsion concepts have been receiving a considerable attention in recent years [1, 2, 3]. The need for environmentally responsible aviation calls for new propulsion concepts that use less fuel and produce less emissions. Hybrid electric propulsion could become a possibility for environmentally responsible aviation. In the future, hybrid electric and all-electric propulsion commercial aircraft could become a viable option. One such concept is distributed propulsion aircraft that employ several small propulsion units, or propulsors, powered by gas turbine generators [1, 2, 3]. Advanced concepts of distributed propulsion aircraft using the boundary layer ingestion have been investigated recently [4]. Drag reduction concepts via electric distributed propulsion have been studied [5]. Due to the relatively small size, distributed propulsion could be powered by electric motors to drive a single-stage or multi-stage fan for thrust production. Power is generated by a gas turbine generator which could be a core power-producing gas turbine engine without a thrust-producing turbofan. Power distribution systems could be efficiently designed to supply electricity to the distributed propulsors.

Aeroelastic wing shaping control refers to the exploitation of aeroelasticity of a flexible wing structure by shape changing control in order to achieve a net beneficial effect on aircraft performance, stability, or control [6]. The wing warping method employed by the Wright brothers for flight control of the Wright flyer in the beginning of the aviation history in the United States is in effect one of the early aeroelastic wing shaping control concepts [7]. The U.S. Air Force / NASA Active Aeroelastic Wing (AAW) program in the late 1990's developed a technology for roll control through the use of wing twist or warping which was demonstrated on a F-18 aircraft modified to reduce the wing stiffness [8]. Wing warping concepts such as those employed by the Wright brothers and the AAW program demonstrate the potential use of aeroelastic wing shaping control for aircraft flight control.

---

[1]Research Scientist, NASA Ames Research Center, Intelligent Systems Division, Building N-269, Moffett Field, 94035, AIAA Associate Fellow

[2]Aerospace Engineer, NASA Ames Research Center, Intelligent Systems Division, Building N-269, Moffett Field, 94035

[3]Aerospace Engineer, NASA Ames Research Center, Intelligent Systems Division, Building N-269, Moffett Field, 94035

[4]Student Intern, Universities Space Research Association, Intelligent Systems Division, Building N-269, Moffett Field, 94035

Without addressing aeroelasticity explicitly, many wing morphing concepts have been developed throughout the history of aviation. Wing morphing includes many methods whereby a wing shape is actively controlled via a camber change, an airfoil profile change, or a twist control. Many of these concepts employ novel actuation mechanisms internal to a wing structure without the use of flap mechanisms but in many cases do not address explicitly wing aeroelasticity. One such concept employs a twist control of multiple individual wing sections that comprise a wing structure and are constructed from a digital lattice material [9]. Other wing morphing concepts employ technologies to change only the trailing edge or leading edge areas. One such technology is demonstrated by NASA / U.S. Air Force Adaptive Compliant Trailing Edge project which conducted a flight experiment in 2012 on a Gulfstream III aircraft with a modified trailing edge flap based on a patented technology by Flexsys, Inc [10]. Another similar technology is the pressure adaptive honeycomb which has been demonstrated as a potential morphing concept for adaptive trailing edge mechanisms [11]. Perhaps the most well-known wing morphing concept without explicitly accounting for wing aeroelasticity is the U.S. Air Force Mission Adaptive Wing program which conducted a flight experiment in the 1980's on a F-111 aircraft to demonstrate a variable camber trailing edge technology [12]. There are other studies of wing morphing that take into account aeroelasticity of the wing design. One concept proposes distributed structural actuation of outboard wing sections using actuated ribs [13].

The Variable Camber Continuous Trailing Edge Flap (VCCTEF) concept is a recent example of aeroelastic wing shaping control technology developed by NASA in 2010 [14]. Originally conceived as a control actuation method for exploiting wing aeroelasticity for drag reduction, the VCCTEF employs multiple chordwise segments to create a variable camber surface at the trailing edge, and a continuous trailing edge enabled by a flexible elastomer material to eliminate flap gaps which could otherwise generate viscous drag and noise [15]. Thus, both the spanwise lift distribution and chordwise pressure distribution can be optimized using the VCCTEF as an aeroelastic wing shaping control device. Unlike wing morphing concepts many of which require internal mechanisms, the VCCTEF relies on distributed flap systems for aeroelastic wing shaping control, and thus can be made ready for technology transition to modern passenger transport designs in the near future. The concept was further developed in collaboration with Boeing to implement the VCCTEF on a modern transport wing design [16]. Drag reduction benefits of the VCCTEF have been demonstrated in simulations [17] and experimentally [18]. Aeroelastic modeling of realistic modern transport platforms including NASA Generic Transport Model based on Boeing 757 [19], Common Research Model based on Boeing 777 [20], and next-generation Truss-Braced Wing aircraft equipped with the VCCTEF have been conducted [21].

This study proposes a new aeroelastic wing shaping control concept using distributed propulsion which has been studied under a NASA Aeronautics Research Mission Directorate (ARMD) Seedling Fund Phase I project entitled "Wing Shaping Concepts Using Distributed Propulsion Control For Achieving Optimal L/D to Reduce Fuel Burn" in 2013 [22, 23]. This concept proposes a multidisciplinary aircraft design that leverages wing structural flexibility to gain aerodynamic efficiency through drag reduction for a conventional tube-and-wing aircraft with wing-mounted distributed propulsion. By leveraging wing flexibility, aeroelastic wing shaping control of distributed propulsion aircraft could improve aerodynamic efficiency while maintaining aeroelastic stability. Aeroelastic wing shaping control leverages the ability to introduce aerodynamic forces and moments generated by the distributed propulsors into a wing structure to change its shape. This aeroelastic wing shaping control action can be performed throughout the flight envelope to enable mission-adaptive aircraft performance as the wing shape changes with aircraft gross weight and flight conditions during cruise.

By reducing the wing structural stiffness, the study identifies an improvement in the lift-to-drag ratio L/D as compared to a stiff wing design across a mission profile consisting of a minimum fuel climb, cruise, and continuous descent. The reduction in fuel burn can be attributed to the drag reduction throughout the flight envelope by actively tailoring the spanwise lift distribution using distributed propulsion to change the wing shape. The proposed concept exploits synergistic interactions between lightweight materials, electric distributed propulsion, and active aeroelastic control for reducing the environmental impact of future distributed propulsion aircraft. Aeroelastic wing shaping control is achieved using propulsors distributed along the wing span to provide aircraft flight control and change the wing shape. Aircraft flight control for distributed propulsion aircraft can therefore be designed in a multidisciplinary fashion that leverages the interactions of aircraft flight mechanics, aeroelasticity, and propulsion to achieve improved aircraft performance, stability, and control.

2 Description of Wing Shaping Concept for Distributed Propulsion Aircraft

Distributed propulsion for transport aircraft could pose a new opportunity to meet future environmentally responsible aviation requirements for reduced fuel burn and emissions. Since currently an electric propulsor could only produce a fraction of the thrust output of a typical gas turbine engine, future hybrid electric propulsors are expected to be smaller in size. As such, a distributed propulsion aircraft would need several of these propulsors to be used in a distributed fashion to produce sufficient thrust requirements for take-off, cruise, and landing. These propulsors could be powered by a gas-turbine generator which generates the electricity to drive the propulsors.

Wing-mounted distributed propulsion is a natural consideration for distributed propulsion aircraft. Distributed propulsion

for a conventional tube-and-wing aircraft will require a necessary consideration of aeroelasticity to account for propulsion interactions with the wing structure. The concept of generalized force is associated with the effective force acting on a structure for a given structural dynamic mode shape. The static deflection shape of a cantilever wing structure generally increases monotonically from the wing root to the wing tip. Thus, as thrust is applied further away from the wing root, the generalized force also increases. If not carefully considered, the increase in the thrust force can cause an undesired wing twist that could result in sub-optimal lift distributions at cruise and a potential tip stall during fast maneuvers. An important example is the NASA Helios aircraft that crashed due to the aeroelastic effects not fully accounted for in the flight control laws. The crash of the Helios aircraft was attributed to many factors including complex aero-propulsive-elastic interactions with rigid-body flight dynamics [24].

The concept of generalized stiffness is associated with the effective stiffness of a structure. As the pitching moment created by a thrust force causes a wing section to twist, the orientation of the thrust vector also changes. This results in a force-follower effect that creates a thrust-induced stiffness. Thus, the thrust-induced generalized stiffness associated with distributed propulsion depends on the placement of the propulsors as well as the mode shape. If not carefully considered, the thrust-induced stiffness could adversely affect the divergence speed.

The concept of generalized mass is associated with the effective mass of a structure. Distributed propulsion results in the placement of the propulsors along the wing span. Thus, the generalized mass associated with distributed propulsion depends on the placement of the propulsors as well as the mode shape. As the propulsors are placed outboard of the aircraft wings, the generalized mass contribution increases. This causes the natural frequencies of a wing structure to decrease. If not carefully considered, changes in the generalized mass and stiffness could adversely affect the flutter speed. Aircraft are designed to meet flutter certification requirements for safety consideration.

The virtual work principle can be applied to compute the generalized force, mass and stiffness of a given structure. The concept of distributed propulsion can be leveraged to alter the generalized force, mass, and stiffness of a wing structure advantageously in connection with aeroelastic wing shaping control for the benefit of improved aerodynamic performance of a flexible wing aircraft. This study examines a fuel-optimal performance during climb, cruise, and continuous descent that accounts for wing aeroelasticity and optimal thrust distribution along the wing span. The propulsive forces and moments produced from the distributed propulsors mounted along the wing span can be used to optimize L/D by modifying the wing twist and bending.
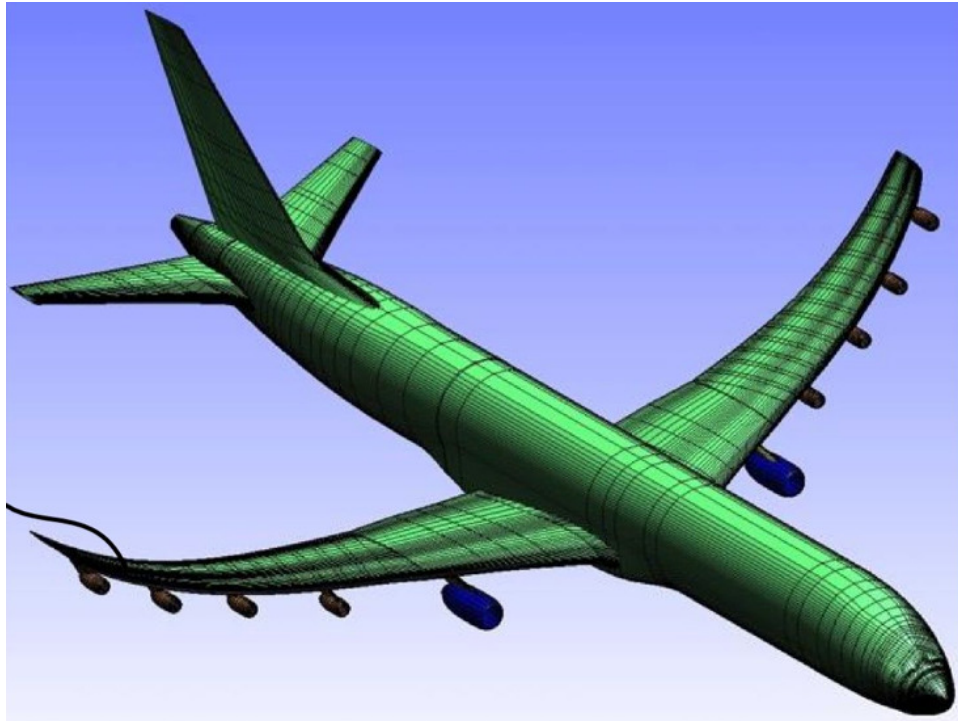

Figure 1: Distributed Propulsion Aircraft with Wing Shaping Control

Figure 1 illustrates one concept of a conventional transport aircraft having an inboard turbofan engine core which serves as a generator to provide power to the distributed propulsors which could be electric fans along the wing span. It should be noted that a variety of configurations of differing numbers and locations of generators and propulsors, extent of thrust, and nacelle sizes, and placement along the wing span either above or below the wing as well as along the chordwise direction forward

near the wing leading edge or aft near the wing trailing edge could be employed. All of these configurations can be considered in a distributed propulsion aircraft multidisciplinary design optimization (MDO) to meet applicable requirements for flight performance, stability, and control. Thus, the illustrated placement of the generator and distributed propulsors below the wings near the leading edge is just one possible concept. As the wing flexibility increases, the thrust distribution can be leveraged to change the wing local angle of attack in order to re-optimize the lift distribution for improved aerodynamic efficiency. The propulsors placed near the wing tip typically produce a larger generalized force for aeroelastic wing shaping control. On the other hand, the propulsors placed closer to the wing root produce no increase in the generalized mass and therefore may be more favorable for aeroelastic stability from the flutter and divergence standpoints. Therefore, the placement of the propulsors can have a profound impact on the aeroelastic behaviors of a flexible wing and the overall aerodynamic performance of a distributed propulsion aircraft. With careful consideration, the aeroelastic behaviors can be tailored in a favorable manner with a suitable placement of the propulsors in the MDO process.

A typical MDO process includes propulsor sizing, propulsor placement, wing structural design with mass and stiffness tailoring, wing aerodynamics with propulsion interactions, and aircraft flight control. All of these attributes must be integrated to achieve the overall aircraft performance, stability, and control requirements. For a distributed propulsion layout and a given wing planform, wing torsion and bending stiffness properties can be optimized for both weight reduction and optimal lift distribution at a design cruise condition by exploiting the aero-propulsive-elastic interactions for aerodynamic benefits. The ability to exploit aero-propulsive-elastic interactions depends on how flexible a wing structure can be made. For optimization studies, an aero-propulsive-elastic model can be coupled with an aircraft aerodynamic model to assess the aircraft L/D performance. The wing stiffness, jig-shape twist distribution, and thrust distribution are tailored in a synergistic manner to achieve an optimal lift distribution in the presence of distributed propulsion.

For under-wing mounted propulsion, a positive nose-up twist is generated. On the hand, the aeroelastic wash-out twist due to bending and torsion is normally negative nose-down for a swept-back wing. Thus, the jig-shape twist, that is the geometric twist of a wing during the manufacturing process, must be designed to account for the positive twist due to under-wing mounted distributed propulsion. This would imply a more negative nose-down jig-shape twist. Current transport aircraft typically has a wash-out jig-shape twist that varies from positive at the wing root to negative at the wing tip. With under-wing mounted distributed propulsion, depending on the wing stiffness and thrust distribution, a typical jig-shape twist could be tailored to have more negative twist at the wing tip. The converse is true for over-wing mounted distributed propulsion which creates a negative nose-down twist. In this case, the jig-shape twist could be tailored to have less negative nose-down twist. Thus, the wing stiffness, jig-shape twist distribution, thrust distribution, and placement of the distributed propulsors are to be designed in an integrated and synergistic manner by employing an aero-propulsive-elastic model to account for the multidisciplinary interactions. Any of these design parameters can be exploited in the design to attain maximum aerodynamic benefits by taking advantage of the aeroelastic wing shaping control.

In this conceptual study, it is of interest to consider distributed propulsion aircraft aerodynamics, wing aeroelastic tailoring for optimal L/D, distribution propulsion sizing and placement, flutter analysis, and mission performance analysis to quantify the fuel reduction benefit. The study is limited to ducted fan propulsors. Additionally, it is of interest to consider flight control requirements with differential thrust control, vertical tail sizing for the engine-out take-off condition, and the overall system architecture and desired benefits. A MDO framework can be developed that includes aircraft geometry, aerodynamics, propulsion, wing structure, aero-propulsive-elasticity, stability, flight control, and system analysis.

2.1   Aerodynamics

The baseline aircraft model is the NASA Generic Transport Model (GTM) which has a similar planform as the Boeing 757 aircraft equiped with conventional turbofan engines as shown in Fig. 2. The distributed propulsion aircraft is modified from the baseline GTM by replacing the turbofan engines with four propulsors and one generator per wing, referred to as single-generator distributed propulsion aircraft, and two generators per wing, referred to as dual-generator distributed propulsion aircraft. The generators which are essentially a gas turbine engine core generate power to drive the propulsors which are modeled as electric fans. For the single-generator configuration, the four propulsors are positioned along the normalized wing stations $\eta = \frac{2y}{b} = 0.3624$ for propulsor 1 closest to the wing root, $\eta = 0.5636$ for propulsor 2, $\eta = 0.7648$ for propulsor 3, and $\eta = 0.9660$ for propulsor 4 where y is the wing station along the aircraft pitch axis and b is the wing span which is about 124 ft for the GTM. For the dual-generator configuration, the locations of the propulsors are at the normalized wing stations $\eta = 0.3222$ for propulsor 1, $\eta = 30.0169$ for propulsor 2, $\eta = 0.8051$ for propulsor 3, and $\eta = 0.9660$ for propulsor 4. All the propulsors are placed below the wing with a vertical offset of 2 ft between the thrust centers of the propulsors and the elastic axis of the wing. The propulsors are sized to produce the same total thrust as that of the baseline GTM which is equal to 44,000 lbs per engine. For the single-generator configuration, the generators are placed at the normalized wing station $\eta = 0.1613$. For the dual-generator configuration, the turbo-generators are located at the normalized wing stations $\eta = 0.1613$ and $\eta = 0.6442$. All the generators are placed below the wing with a vertical offset of 3 ft between the geometric centers of the generators and the elastic axis of the wing. For comparison, the turbofan engines for the baseline GTM are at the normalized wing station

$\eta = 0.3461$.

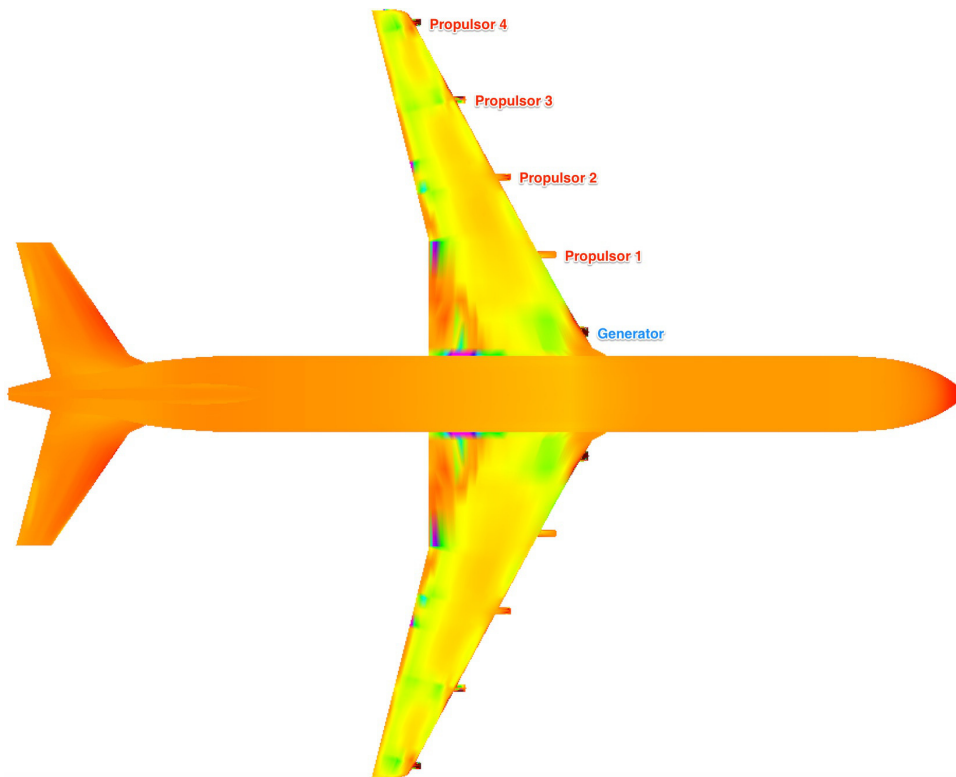Figure 2: NASA Generic Transport Model (GTM)

Figure 3: Pressure Distribution of Single-Generator Distributed Propulsion Aircraft

It should be noted this study examines the gas turbine generators as a power generation option. This option is well within the current and near-term aircraft technology capabilities. A farther-term option is to rely solely on batteries as a power

source. A hybrid option of gas-electric propulsion is also a possibility. The approach in this study can be applied to alternative sources of power such as batteries or gas-electric propulsion with a suitable modification of the various distributed propulsion configurations and the inclusion of battery weight into the aircraft model.

Figures 3 and 4 show the computational results of the pressure distribution of the single-generator and dual-generator distributed propulsion aircraft concepts, respectively, using vortex-lattice code Vorlax for rapid conceptual aerodynamic analysis. Aerodynamic performance in terms of lift, drag, and pitching moment is generated by Vorlax. Additionally, the lift distribution which is an important quantity for aeroelastic analysis is also computed. This information is used in the aero-propulsive-elastic analysis.
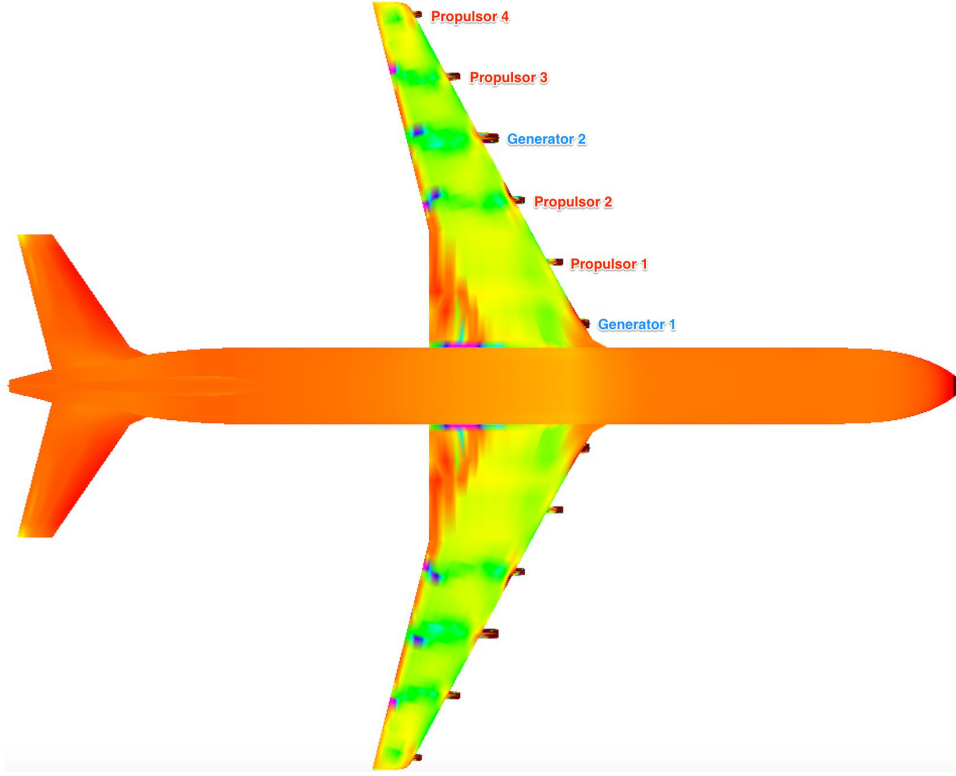
Figure 4: Pressure Distribution of Dual-Generator Distributed Propulsion Aircraft

2.2 Propulsion Performance Analysis

A fan performance analysis is performed to determine the relationships between thrust and weight for a given fan diameter and pressure ratio. These relationships are then used to determine the fan size needed to achieve the take-off thrust required for the distributed propulsion aircraft. Once these factors are determined, it is possible to calculate parameters for a ducted fan propulsor. Given a fan total pressure ratio and a fan isentropic efficiency, the total temperature ratio can be computed as [25]

$$\frac{T_{0_2}}{T_{0_1}} = \lambda^{\frac{\gamma-1}{\eta\gamma}} \tag{1}$$

where T_{0_1} and T_{0_2} denote the inlet and exit total temperatures, respectively, λ is the fan total pressure ratio, γ is the specific heat constant typically equal to 1.4 for diatomic gases including air, and η is the fan isentropic efficiency.

For a constant area duct and assuming a uniform flow with zero inlet and exit swirls to minimize the kinetic energy loss, the continuity equation can be used to determine the exit Mach number as [26]

$$\dot{m} = \sqrt{\frac{\gamma}{RT_{0_1}}} P_{0_1} A M_1 \left(1 + \frac{\gamma-1}{2}M_1^2\right)^{-\frac{\gamma+1}{2(\gamma-1)}} = \sqrt{\frac{\gamma}{RT_{0_2}}} P_{0_2} A M_2 \left(1 + \frac{\gamma-1}{2}M_2^2\right)^{-\frac{\gamma+1}{2(\gamma-1)}} \tag{2}$$

where $\dot{m}$ is the mass flow rate, P_{0_1} and P_{0_2} are the inlet and exit total pressures, respectively, and A is the fan area.

The net thrust force produced by a fan is computed as

$$T = (P_2 - P_1)A + \dot{m}(V_2 - V_1) \tag{3}$$

6

where P_1 and P_2 are the inlet and exit static pressures, respectively, and V_1 and V_2 are the inlet and exit velocities, respectively.

The power requirement is computed as

$$\dot{W} = \dot{m} c_p \left(T_{0_2} - T_{0_1} \right) \tag{4}$$

where c_p is the constant-pressure specific heat ratio.

All fan performance parameters are then corrected to the standard sea-level condition by the corrected pressure ratio $\delta = \frac{P_{0_1}}{P_{SL}}$ and temperature ratio $\theta = \frac{T_{0_1}}{T_{SL}}$ where $P_{SL} = 2116.2$ psf and $T_{SL} = 518.69°$R are the standard pressure and temperature at sea level. The corrected thrust, mass flow rate, and power are then computed as

$$\dot{m}_c = \frac{\dot{m}\sqrt{\theta}}{\delta} \tag{5}$$

$$T_c = \frac{T}{\delta} \tag{6}$$

$$\dot{W}_c = \frac{\dot{W}}{\delta\sqrt{\theta}} \tag{7}$$

The fan total pressure ratio is assumed to be 1.8 with a fan isentropic efficiency of 90% at 35,000 ft and Mach 0.8. In general, the fan total pressure ratio and isentropic fan efficiency will both change depending on the mass flow rate. By assuming a quadratic relationship between the fan total pressure ratio and the corrected mass flow rate per unit area, relevant parameters can be determined as a function of the corrected mass flow rate per unit area. Therefore

$$\lambda = 1 + c \left(\frac{\dot{m}_c}{A} \right)^2 \tag{8}$$

where c is a parameter to be determined. Using a fan diameter of 10 ft and a hub-to-tip ratio of 0.35, this gives $c = 0.3656$.

A linear relationship is assumed between fan total pressure ratio and isentropic fan efficiency according to

$$\eta = a \left(\lambda - 1 \right) \tag{9}$$

where $a = 1.125$ that corresponds to a fan isentropic efficiency of 90% at a design fan total pressure ratio of 1.8.

Using these relationships, the fan isentropic efficiency at off-design pressure ratio is related to the corrected mass flow rate per unit area according to

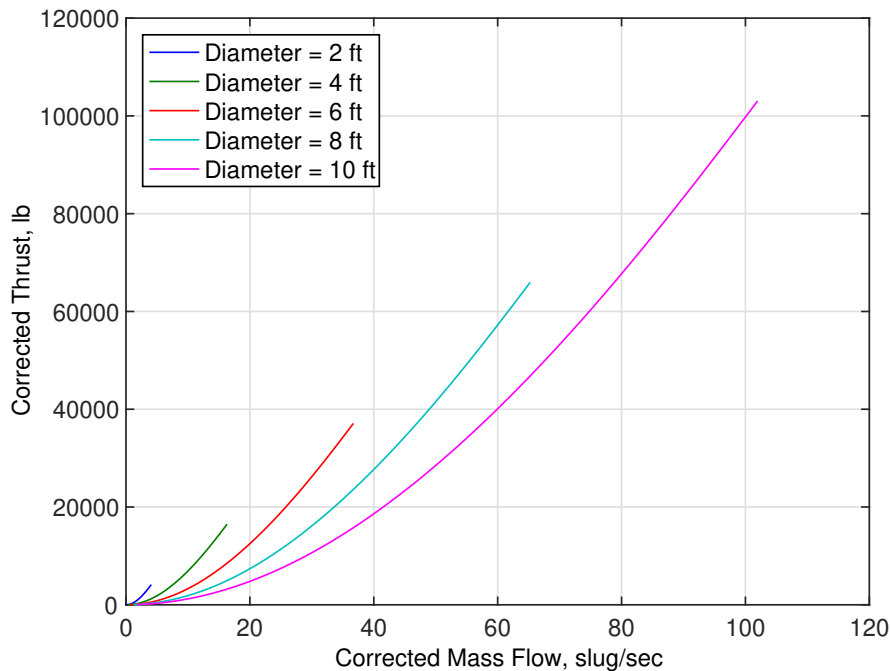$$\eta = ac \left(\frac{\dot{m}_c}{A} \right)^2 \tag{10}$$

Figure 5: Corrected Thrust as Function of Corrected Mass Flow Rate

Figure 5 is the plot of the corrected thrust as a function of the correct mass flow rate for various fan diameters. As the fan diameter increases, the corrected thrust and mass flow rate increase accordingly. Figure 6 illustrates the corrected thrust as a function of the fan diameter for various fan total pressure ratios. As the fan pressure ratio increases, the corrected thrust also increases accordingly.
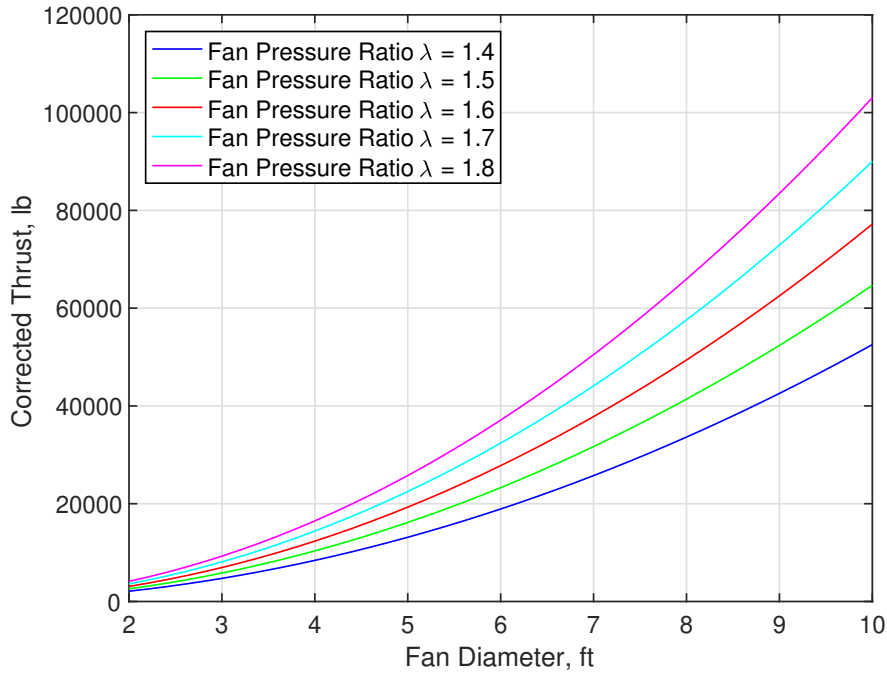

Figure 6: Corrected Thrust as Function of Fan Diameter

To validate the fan performance model, publicly available data from five commercial turbofan engines are used. These are shown in Table 1.

Table 1: Turbofan Engine Data

Engine	Fan Diameter, in	Rated Maximum Thrust, lbs	Estimated Dry Weight, lbs
Pratt-Whiney PW2000 [27]	78.5	43,000	5,876
Rolls-Royce Trent 700 [28]	97.4	71,100	7,481
Rolls-Royce Trent 1000 [29]	112	74,000	11,307
Engine Alliance GP7200 [30]	116.7	81,500	14,206
General Electric GE90 [31]	128	127,900	12,705

Figure 7 is the plot of the rated maximum corrected thrust as a function of the fan diameter. For the analysis, it is assumed that the residual thrust of the gas turbine engine core for high-bypass turbofan engines is negligible. The data are curvefitted using a second-order polynomial. Based on curve fitting, the relationship between the corrected thrust and the fan diameter agrees quite well. Figure 8 is the plot of the estimated fan weight not including the gas turbine engine core as a function of the fan diameter. Thus, for a given fan diameter and fan total pressure ratio, one can determine the maximum corrected thrust from Fig. 6 and fan weight from Fig. 8. The relationship between the fan dry weight and the fan diameter is then obtained empirically as

$$W_f = d_f \left(102.6827 d_f + 228.0575 \right) \tag{11}$$

where W_f is the fan dry weight in pounds and d_f is the fan diameter in feet.

The conventional GTM without distributed propulsion is powered by two turbofan engines, each with a maximum rated thrust of 44,000 lbs. Each turbofan engine weighs 11,500 lbs. Using Figs. 7 and 8, the fan diameter of the turbofan without the engine core is estimated to be 6.5339 ft. This results in a dry weight of 5,874 lbs. The weight of the engine core is then computed to be 5,626 lbs.
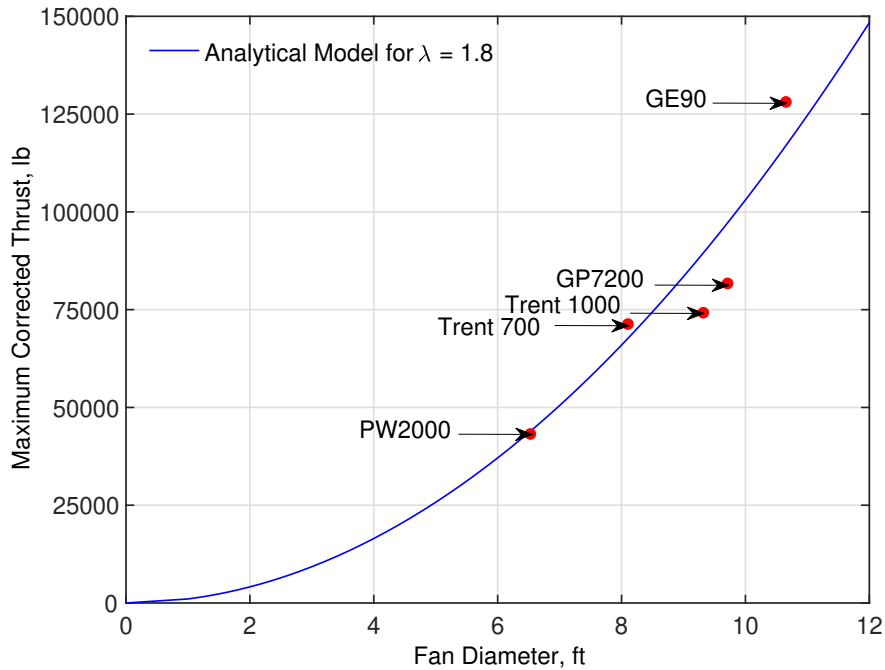
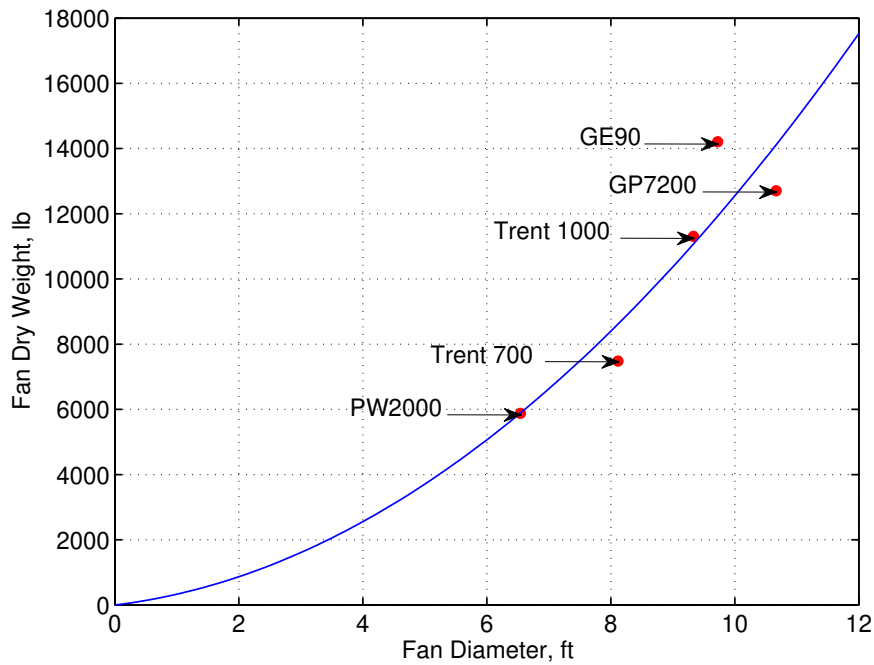Figure 7: Maximum Corrected Thrust vs. Fan Diameter for Commercial Turbofan Engines

Figure 8: Estimated Fan Weight vs. Fan Diameter for Commercial Turbofan Engines

With distributed propulsion, assuming that the generator does not produce thrust and is essentially the engine core of the turbofan above for a single-generator configuration, then each propulsor needs to produce 11,000 lbs of thrust if four propulsors are used. From Figs. 7 and 8, these propulsors would have a fan diameter of 3.2659 ft and a dry weight of 1,840 lbs. The total weight of the distributed propulsion system is then equal to 12,986 lbs which is larger than the weight of the turbofan engine above by about 18%.

This analysis is only approximate. However, it may point out that the weight consideration must be taken into account since the total weight of a distributed propulsion system may be larger than that of a single turbofan engine. This weight penalty may offset any aerodynamic benefit of distributed propulsion.

2.3 Aero-Propulsive-Elasticity

Wing aeroelasticity is modeled by the flapwise bending deflection $w(x,t)$ and torsional twist $\theta(t)$ using the classical beam theory which is suitable for high aspect ratio wings with moderate sweep angles typical of modern transport aircraft. Let x be the coordinate along the wing elastic axis as illustrated in Fig. 9, then the aeroelastic equations are given by [32, 33, 34]

$$m\frac{\partial^2 w}{\partial t^2} - me_{cg}\frac{\partial^2 \theta}{\partial t^2} + \frac{\partial^2}{\partial x^2}\left(EI_{yy}\frac{\partial^2 w}{\partial x^2}\right) = -mg\cos\Lambda + f_z^a + f_z^p - \frac{\partial m_y^a}{\partial x} - \frac{\partial m_y^p}{\partial x} \tag{12}$$

$$I_{xx}\frac{\partial^2 \theta}{\partial t^2} - me_{cg}\frac{\partial^2 w}{\partial t^2} - \frac{\partial}{\partial x}\left(GJ\frac{\partial \theta}{\partial x}\right) = mge_{cg}\cos^2\Lambda + m_x^a + m_x^p \tag{13}$$

where EI and GJ are the bending and torsional stiffness values, m is the distributed mass, e_{cg} is the mass offset from the elastic axis (positive when the center of mass is aft of the elastic axis), I_{xx} is the distributed mass polar moment of inertia, and Λ is the sweep angle of the elastic axis.
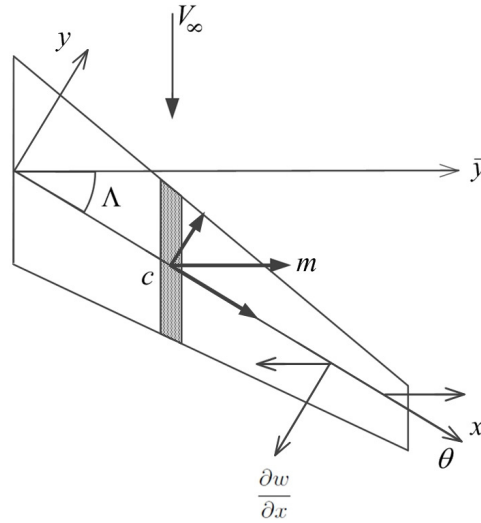
Figure 9: Local Wing Elastic Reference Frame

The aerodynamic lift force and moments which include both steady and unsteady aerodynamic contributions can be expressed as

$$f_z^a = c_L q_\infty c \cos\Lambda + l^{nc}\cos\Lambda \tag{14}$$

$$m_x^a = c_m q_\infty c^2 \cos^2\Lambda + m^{nc}\cos^2\Lambda \tag{15}$$

$$m_y^a = -c_m q_\infty c^2 \cos\Lambda\sin\Lambda - m^{nc}\cos\Lambda\sin\Lambda \tag{16}$$

where q_∞ is the dynamic pressure and c is the section chord in the streamwise direction.

The unsteady lift and pitching moment coefficients in the streamwise direction can be modeled by the Theodorsen's theory [35] as

$$c_L = c_{L_r} + C(k)c_{L_\alpha}\left(\theta\cos\Lambda - \frac{\partial w}{\partial x}\sin\Lambda + \frac{e_c\cos\Lambda}{V_\infty}\frac{\partial \theta}{\partial t} - \frac{1}{V_\infty}\frac{\partial w}{\partial t}\right) \tag{17}$$

$$c_m = c_{m_{ac}} + c_L\frac{e}{c} \tag{18}$$

where c_{L_r} is the rigid-wing lift coefficient in the streamwise direction, $c_{m_{ac}}$ is the rigid-wing pitching moment coefficient about the aerodynamic center, e is the offset of the aerodynamic center from the elastic axis (positive when the aerodynamic center is forward of the elastic axis), e_c is the offset of the three-quarter-chord point from the elastic axis (positive when the three-quarter-chord point is aft of the elastic axis), and $C(k)$ is the Theodorsen's function for unsteady aerodynamics where $k = \frac{\omega c}{2V_\infty}$ is the reduced frequency and ω is the frequency of the harmonic motion of an airfoil.

10

The non-circulatory force and moments are given by

$$l^{nc} = \rho_\infty \frac{\pi c^2}{4} \left(V_\infty \cos\Lambda \frac{\partial\theta}{\partial t} + e_m \cos\Lambda \frac{\partial^2\theta}{\partial t^2} - \frac{\partial^2 w}{\partial t^2} \right) \tag{19}$$

$$m^{nc} = -\rho_\infty \frac{\pi}{4} c^2 e_m \left(e_m \frac{\partial^2\theta}{\partial t^2} \cos\Lambda - \frac{\partial^2 w}{\partial t^2} \right) - \rho_\infty \frac{\pi c^2}{4} e_c V_\infty \frac{\partial\theta}{\partial t} \cos\Lambda - \rho_\infty \frac{\pi c^4}{128} \frac{\partial^2\theta}{\partial t^2} \cos\Lambda \tag{20}$$

where ρ_∞ is the air density and e_m is the offset of the mid-chord point from the elastic axis (positive is when the mid-chord point is aft of the elastic axis).

The propulsive force f_z^p and moment m_x^p influence wing aeroelasticity for a wing-mounted propulsor. This interaction is due to the force follower effect. In other words, the thrust force and moment cause the wing to twist and bend. In turn, the wing elasticity generates a restoring force to oppose the aeroelastic deflections caused by the thrust force and moment. The net result is that the wing stiffness is affected by the thrust force and moment. This is called thrust-induced stiffness.

The propulsive force and moments are given by

$$f_z^p = \sum_{i=1}^{n} \delta\left(x - x_i\right) \left(-m_i \frac{\partial^2 w}{\partial t^2} - m_i y_i \frac{\partial^2\theta}{\partial t^2} - m_i g - T_i \sin\Lambda \frac{\partial w}{\partial x} + T_i \cos\Lambda\theta \right) \tag{21}$$

$$m_x^p = \sum_{i=1}^{n} \delta\left(x - x_i\right) \left[-I_i \frac{\partial^2\theta}{\partial t^2} - m_i y_i \frac{\partial^2 w}{\partial t^2} - m_i g y_i - T_i \sin\Lambda \frac{\partial w}{\partial x} y_i + T_i \cos\Lambda z_i \right] + \sum_{i=1}^{n} \delta\left(x - \xi\right) \left[-T_i \cos\Lambda\left(x_i - x\right) \frac{\partial w}{\partial x} \right] \tag{22}$$

$$m_y^p = \sum_{i=1}^{n} \delta\left(x - x_i\right) \left(-T_i \sin\Lambda z_i + T_i \sin\Lambda y_i\theta \right) \tag{23}$$

where T_i is the propulsor thrust, m_i is the propulsor mass, I_i is the mass polar moment of inertia of the propulsor, (x_i, y_i, z_i) is the coordinate of the propulsor thrust center such that x_i is the wing station along the elastic axis, $y_i > 0$ forward of the elastic axis, and $z_i > 0$ below the elastic axis, and $\delta\left(x - \xi\right)$ where $0 \leq \xi \leq x_i$ is the Dirac delta function that relates the distributed force f_z^p and moments m_x^p and m_y^p to the concentrated force and moments at $x = \xi$ as

$$\int_0^L \delta\left(x - \xi\right) f\left(x\right) dx = f\left(\xi\right) \tag{24}$$

Figure 10: Static Aeroelastic Deflection of Distributed Propulsion Aircraft

Note that the propulsive force and moments not only are influenced by the thrust force and the propulsor weight but also by the aeroelastic deflections. The aeroelastic deflection-dependent terms give rise to the thrust-induced stiffness. A three-dimensional beam finite-element model is developed for both static and dynamic aero-propulsive-elasticity. The model computes the aeroelastic deflections due to the aerodynamic and propulsive forces and moments, as shown in Fig. 10, as well as the structural dynamic mode shapes and flutter speed.

The aeroelastic wing shaping control analysis is conducted using a coupled analysis framework that includes the propulsion performance model, aerodynamic model, finite-element model, and automated geometry deformation tool that generates new deformed aircraft wing geometry from the output of the finite-element model. This is shown in Fig. 11. The propulsion performance model is used for sizing and weight estimation. The distributed propulsion placement is determined by an aero-propulsive-elastic performance analysis and a flutter analysis to ensure that the candidate placement provides aerodynamic benefits while meeting flutter constraints, especially as the propulsors are placed closer to the wing tip. The aero-propulsive-elastic performance analysis requires an iterative solution method among the aerodynamic model, finite-element model, and propulsion model.
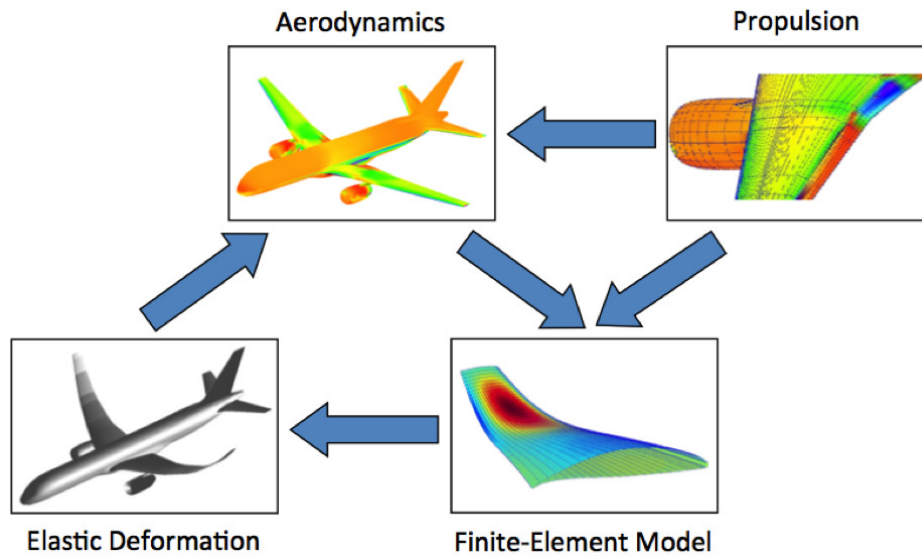
Figure 11: Coupled Aero-Propulsive-Elastic Analysis Framework for Distributed Propulsion Aircraft

3 System Analysis of Distributed Propulsion Aircraft

A preliminary system analysis is conducted to assess the potential benefit of the aeroelastic wing shaping control concept for distributed propulsion aircraft. The following elements are included in the analysis:

3.1 Thrust-Induced Lift

A thrust-induced lift due to the distributed propulsion is generated by leveraging wing aeroelasticity. The pitching moment generated by an under-wing-mounted propulsor causes the wing to twist nose-up. This effectively creates a lift force, called thrust-induced lift. For a swept-back wing, the aerodynamic lift causes the wing to bend upward, thereby creating an effective nose-down wash-out twist that reduces the local angle of attack along the wing span which in turn affects the lift distribution. However, by utilizing the thrust-induced lift, it is possible to compensate for the wash-out twist and to increase the angle of attack in a controlled manner for aerodynamic benefits. Therefore, by leveraging aeroelastic wing shaping control using distributed propulsion, the spanwise lift distribution can be tailored to reduce drag or equivalently increase the aerodynamic efficiency quantity L/D.

Figure 12 illustrates the sensitivity of the thrust-induced lift to the bending stiffness EI and torsional stiffness GJ as a function of the normalized propulsor spacing measured from the wing tip $\Delta\eta = \frac{2\Delta y}{b}$, where Δy is the propulsor spacing along the aircraft pitch axis. The propulsors are mounted below the wing with a vertical offset of 5 ft between the thrust centers of the propulsors and the elastic axis of the wing. For example, for the normalized propulsor spacing $\Delta\eta = 0.2414$ corresponding to a propulsor spacing of 15 ft, The locations of the propulsors are at about $y = 17$ ft for propulsor 1, $y = 32$ ft for propulsor 2, $y = 47$ ft for propulsor 3, and $y = 62$ ft for propulsor 4. As can be seen, the thrust-induced lift increases with a decrease in the torsional stiffness, but decreases with a decrease in the bending stiffness. Reducing torsional stiffness causes the wing to twist

further nose-up, thereby increasing the thrust-induced lift. Reducing the bending stiffness causes an increase in the nose-down wash-out twist which further decreases the thrust-induced lift. Therefore, the torsional stiffness has a more pronounced effect on the thrust-induced lift than the bending stiffness.
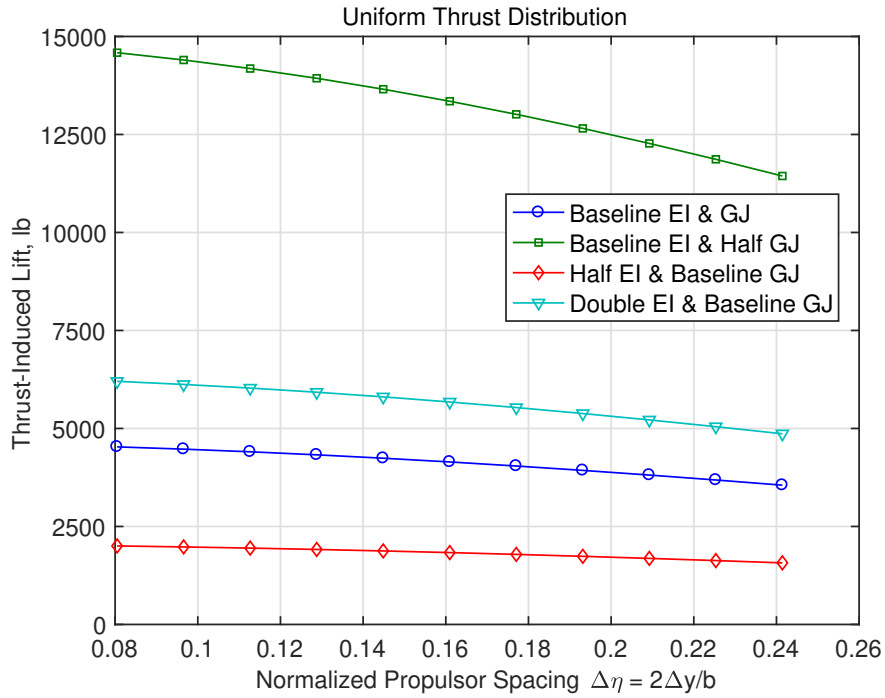

Figure 12: Effect of Stiffness and Propulsor Spacing from Wing Tip on Thrust-Induced Lift for Uniform Thrust Distribution
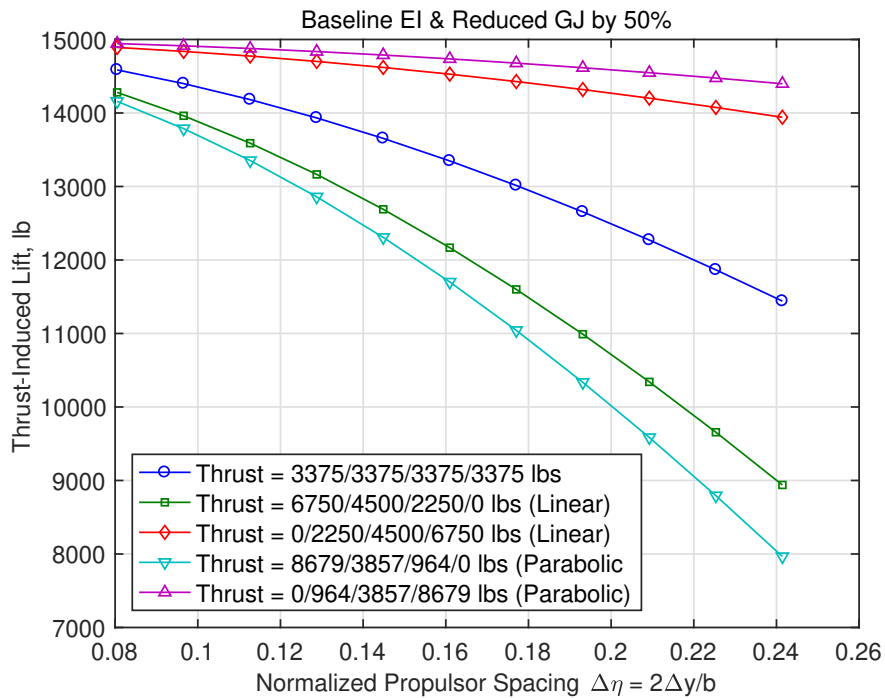

Figure 13: Effect of Thrust Distribution and Propulsor Spacing from Wing Tip on Thrust-Induced Lift

Figure 13 illustrates the thrust-induced lift as a function of the thrust variation along the wing span and the nomalized

propulsor spacing measured from the wing tip. Increasing thrust toward the wing tip results in the largest increase in thrust-induced lift, which amounts to almost 15,000 pounds or 7.5% of the aircraft gross weight. This substantial increase in the thrust-induced lift is accomplished by reducing the torsional stiffness in half and placing the propulsors 5 feet apart starting from the wing tip. Increasing the propulsor spacing from the wing tip has an effect of reducing the thrust-induced lift. The parabolic thrust distribution with the maximum thrust at the wing tip produces the largest thrust-induced lift for a given propulsor spacing.

Recognizing the benefit of the thrust-induced lift by reducing the torsional stiffness, two configurations of the distributed propulsion aircraft are modeled. The stiff wing configuration is with the baseline stiffness. The flexible wing configuration is with the baseline bending stiffness and the reduced torsional stiffness equal to 50% of the baseline value.

3.2 Effect of Aeroelastic Wing Shaping Control on L/D

In Figs. 14 and 15, the spanwise lift distribution at Mach 0.8 and 30,000 ft normalized to the mean aerodynamic chord (MAC) $\bar{c}$ along the normalized wing station η is plotted for the single-generator distributed propulsion aircraft with the stiff wings and flexible wings, respectively, to illustrate the effect of the thrust distribution across the wing span on the lift distribution, hence L/D. The baseline configuration refers to the GTM with two conventional turbofan engines as shown in Fig. 2. The uniform thrust case corresponds to the equal thrust generated by the propulsors. The +50%/+50%/-50%/-50% denotes a 50% increase in thrust of propulsor 1 and propulsor 2 relative to the uniform thrust value and 50% decrease in thrust of propulsor 3 and propulsor 4. The other thrust variations are similarly denoted. The total thrust in all cases is equal to 13,500 lbs at Mach 0.8 and 30,000 ft which corresponds to a uniform corrected thrust of 3,728 lbs per propulsor. Thus, in all the cases, the maximum corrected thrust for the individual propulsors does not exceed 60% of the maximum corrected thrust of 11,000 lbs when the propulsors produce 75% more thrust than the uniform thrust.

In Fig. 15, a triangular shape lift distribution reflects a potentially more structurally efficient lift distribution. An advantageous trade-off can be established between the structural efficiency and aerodynamic efficiency by exploiting the wing flexibility and thrust distribution. This possibility suggests that distributed propulsion can potentially be used for maneuver load alleviation for flexible wing aircraft during maneuvers.

Figures 16 and 17 show the spanwise lift distribution at Mach 0.8 and 30,000 ft normalized to the MAC for the dual-generator distributed propulsion aircraft with the stiff wings and flexible wings, respectively. The lift characteristics of the dual-generator distributed propulsion aircraft are quite similar to those of the single-generator distributed propulsion aircraft.
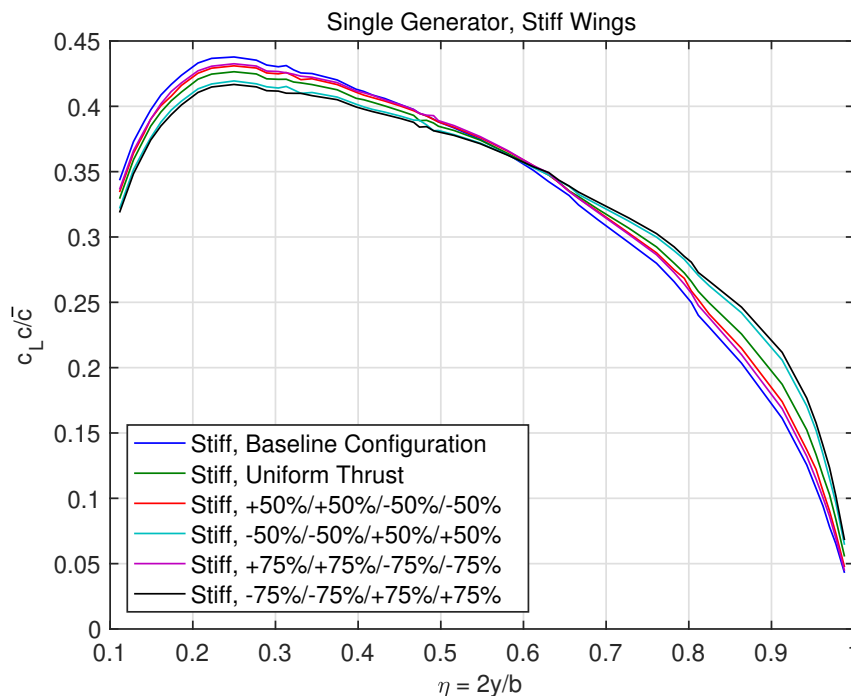

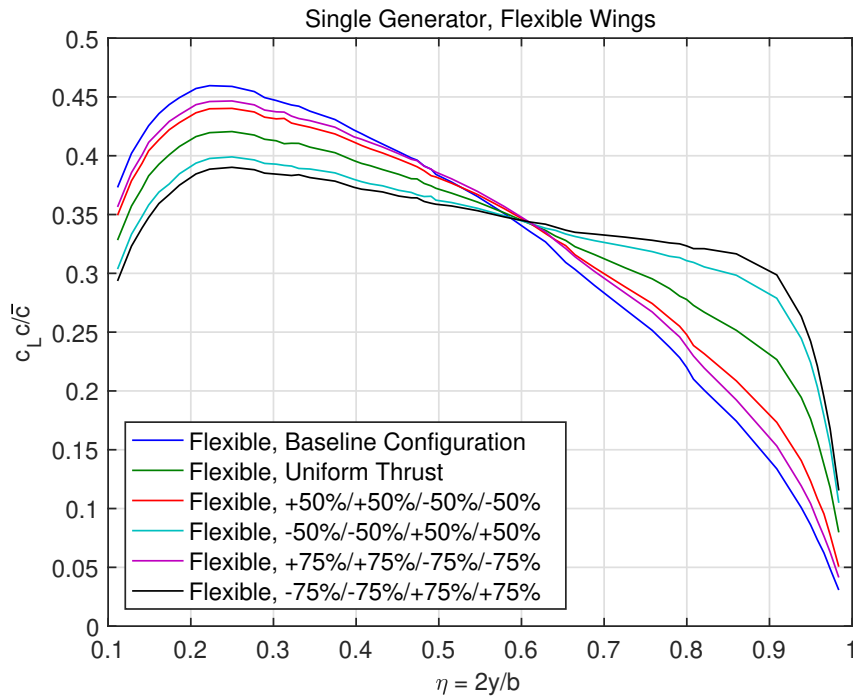Figure 14: Lift Distribution for Single-Generator Distributed Propulsion Aircraft with Stiff Wings

Figure 15: Lift Distribution for Single-Generator Distributed Propulsion Aircraft with Flexible Wings
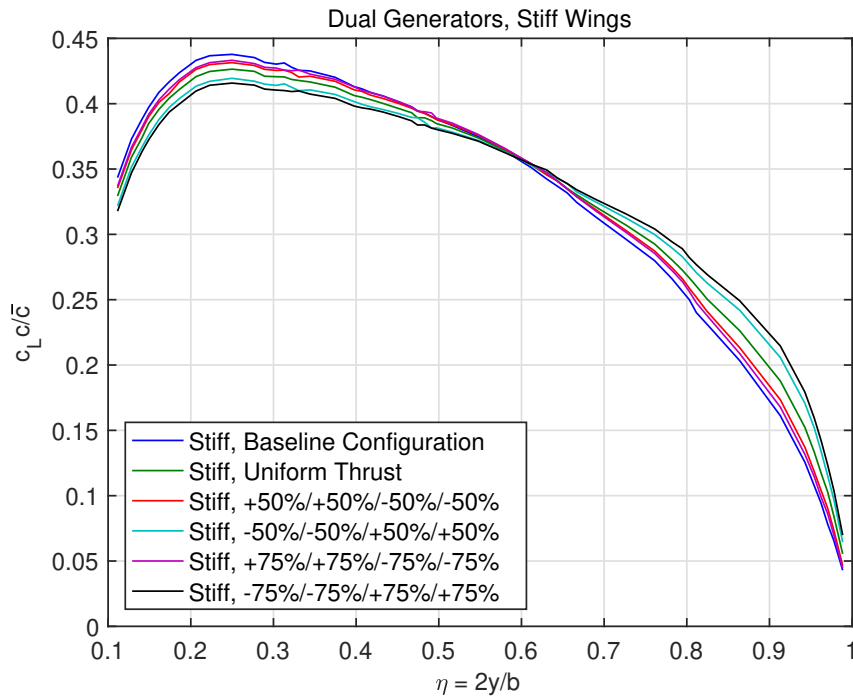

Figure 16: Lift Distribution for Dual-Generator Distributed Propulsion Aircraft with Stiff Wings

In Figs. 18 and 19, the lift coefficient versus the aircraft angle of attack and the drag polar of the single-generator distributed propulsion aircraft with the stiff wings are plotted. The effect of the thrust-induced lift can be seen as the lift coefficients for various thrust distributions are higher than the lift coefficient of the baseline aircraft at a given positive aircraft angle of attack. Increasing the outboard thrust results in higher lift as can be seen in Fig. 18. The drag polars for various thrust distributions which include viscous skin friction drag are similar to one another.
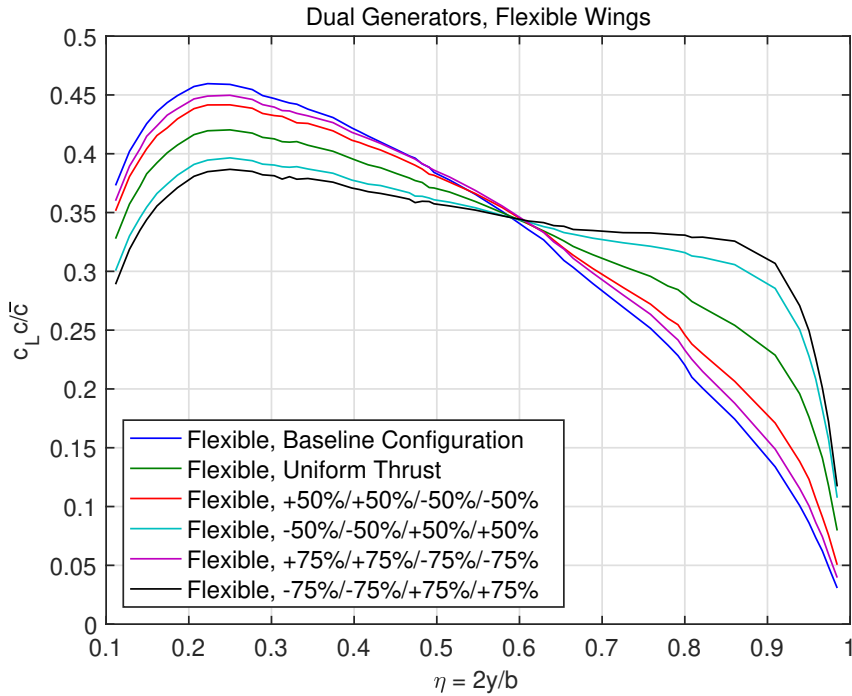
Figure 17: Lift Distribution for Dual-Generator Distributed Propulsion Aircraft with Flexible Wings
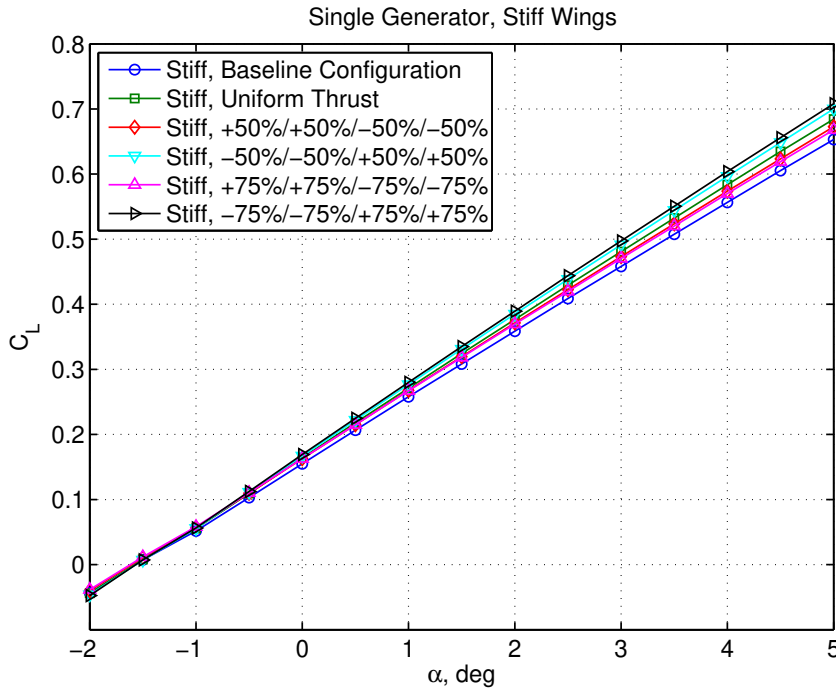
Figure 18: Lift vs. Angle of Attack for Single-Generator Distributed Propulsion Aircraft with Stiff Wings

Figures 20 and 21 are the plots of the lift coefficient versus the aircraft angle of attack and drag polar for the single-generator distributed propulsion aircraft for the flexible wings. The effect of the wing flexibility on the lift coefficient is pronounced as a significant increase in lift is obtained with increasing thrust of the outboard propulsors at a given positive aircraft angle of attack. Correspondingly, the drag coefficient also increases. Thus, increasing thrust of the outboard propulsors causes a reduction in L/D as the local aeroelastic angle of attack increases that causes the lift distribution to deviate from the ideal elliptical lift

16

distribution as shown in Fig. 15. The lift and drag characteristics of the dual-generator distributed propulsion aircraft are very similar to those of the single-generator distributed propulsion aircraft and thus are not plotted.
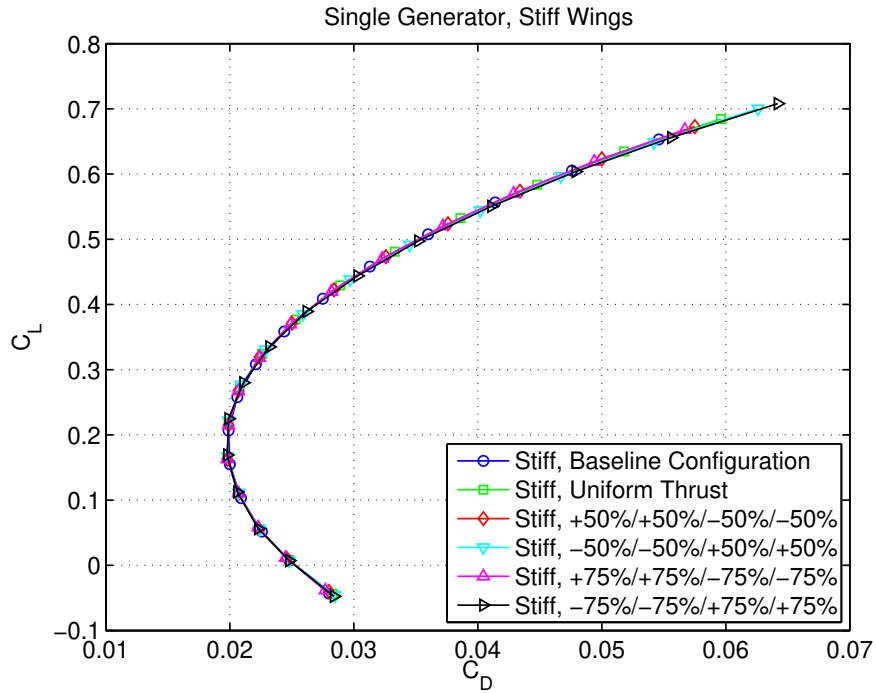
Figure 19: Drag Polar for Single-Generator Distributed Propulsion Aircraft with Stiff Wings
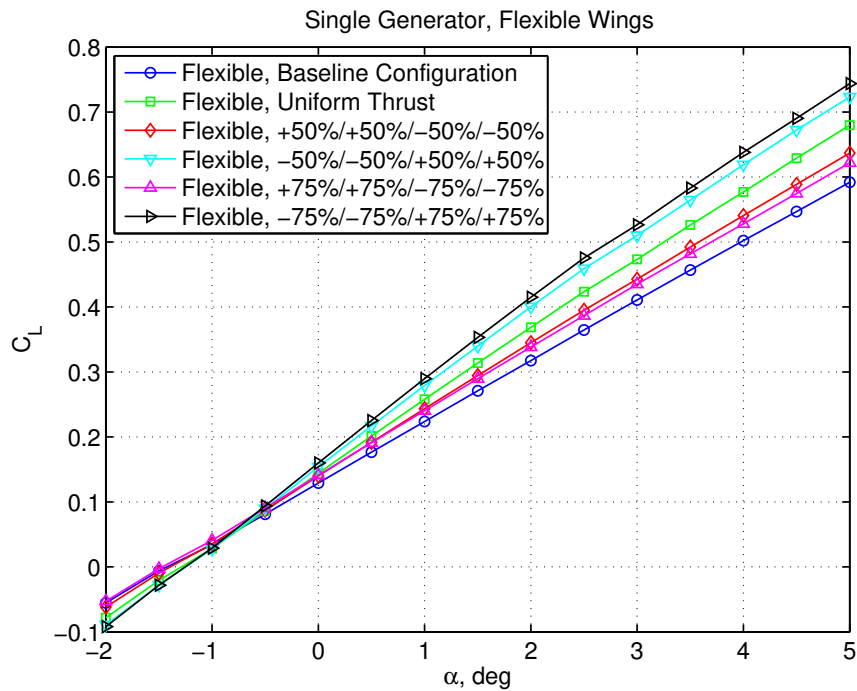
Figure 20: Lift vs. Angle of Attack for Single-Generator Distributed Propulsion Aircraft with Flexible Wings
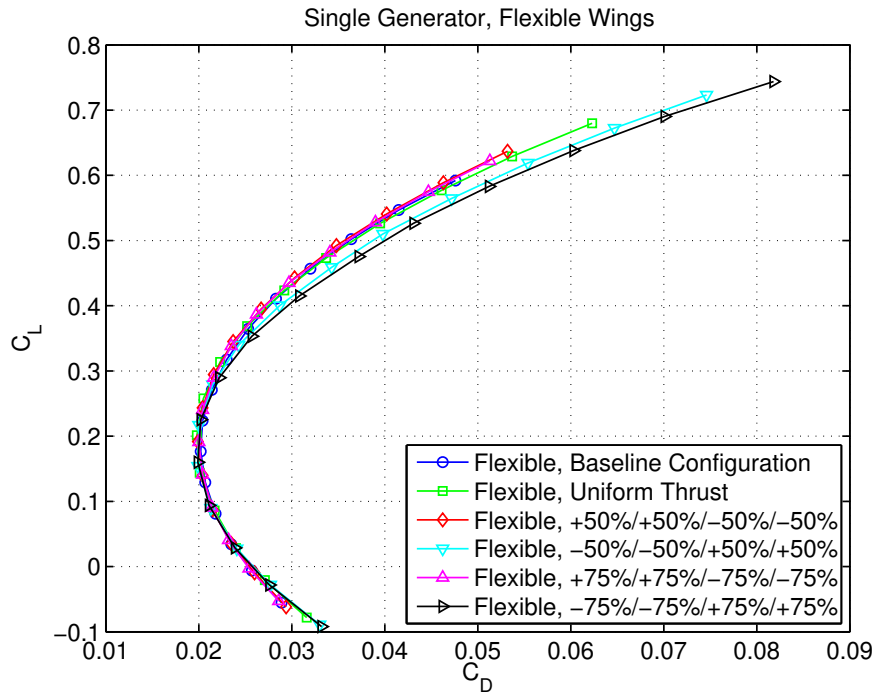
Figure 21: Drag Polar for Single-Generator Distributed Propulsion Aircraft with Flexible Wings

In Figs. 22 and 23, the aerodynamic efficiency or L/D is shown for the single-generator distributed aircraft with the stiff wings and flexible wings. It can be seen that there exist some thrust distributions for which the distributed propulsion aircraft can achieve a higher L/D with flexible wings than with stiff wings for a given positive angle of attack.
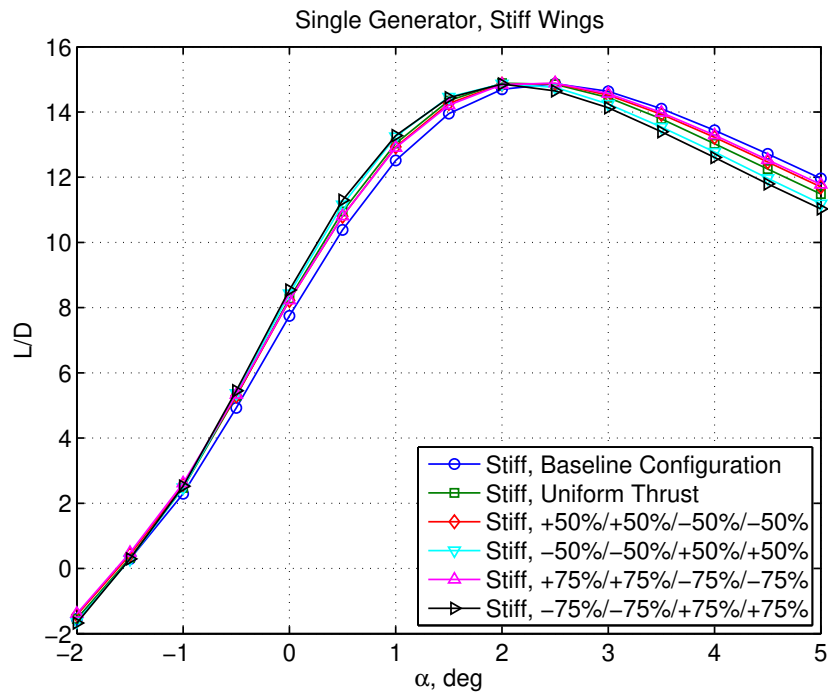
Figure 22: L/D for Single-Generator Distributed Propulsion Aircraft with Stiff Wings

18
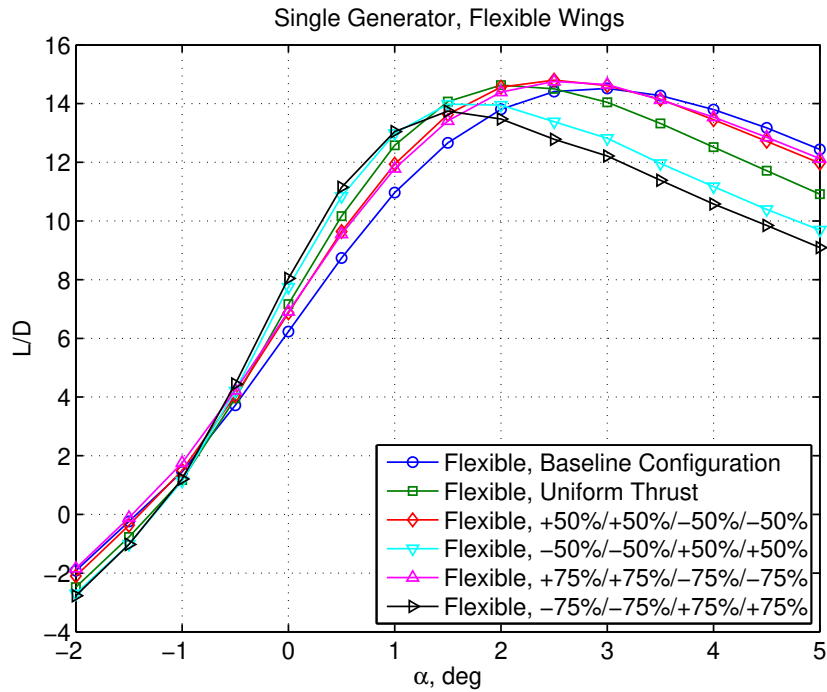
Figure 23: L/D for Single-Generator Distributed Propulsion Aircraft with Flexible Wings

Figures 24 and 25 show the relative improvement in the L/D over the baseline configuration as a function of the angle of attack for the single-generator distributed aircraft with the stiff wings and flexible wings. For a normal angle of attack range at cruise between $1°$ and $2°$, the distributed propulsion aircraft can achieve a better L/D with the flexible wings than with stiff wings.
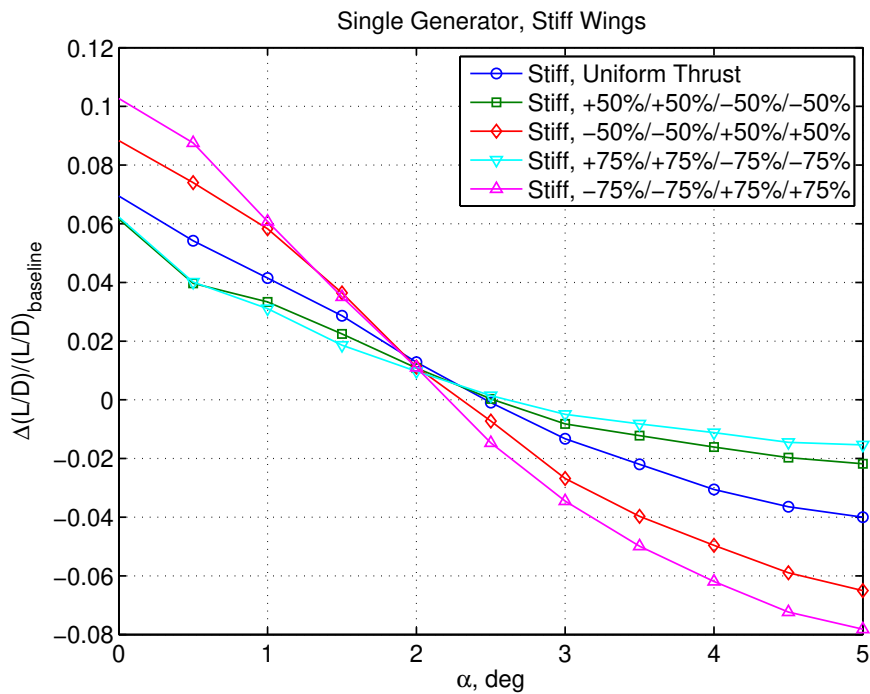
Figure 24: Relative L/D Improvement over Baseline for Single-Generator Distributed Propulsion Aircraft with Stiff Wings
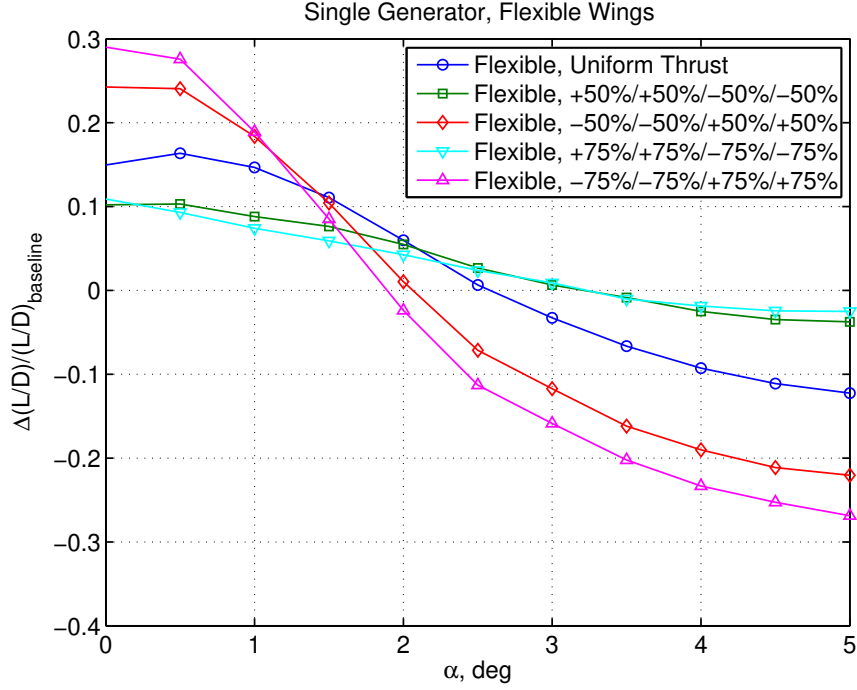
Figure 25: Relative L/D Improvement over Baseline for Single-Generator Distributed Propulsion Aircraft with Flexible Wings

3.3 Performance Analysis

A performance analysis is conducted to evaluate the potential benefits of the aeroelastic wing shaping control concept for distributed propulsion aircraft. A mission profile is considered that includes a climb segment, a cruise segment, and a continuous descent segment. It is assumed that the mission profile takes place only in the vertical plane. For the climb segment, the model uses an operational empty weight of 175,000 pounds carrying 25,000 pounds of fuel, and a maximum thrust climb along an optimal singular arc in the $V - h$ (airspeed and altitude) plane according to the singular arc formula below [36]:

$$f(V,h) = F + V \frac{\partial F}{\partial V} - \frac{V^2}{g} \frac{\partial F}{\partial h} - \frac{FV}{cT} \left[\frac{\partial (cT)}{\partial V} - \frac{V}{g} \frac{\partial (cT)}{\partial h} \right] = 0 \tag{25}$$

where T is the total maximum thrust, g is the gravity constant, F is the specific excess thrust, and c is the thrust-specific fuel consumption.

The specific excess thrust is given by the following formula:

$$F(V,h,W) = \frac{T(V,h) - D(V,h)}{W} \tag{26}$$

where D is the aerodynamic drag and W is the aircraft weight.

The thrust-specific fuel consumption is modeled as a function of the airspeed and altitude, and is given by the following formula:

$$c(M,h) = (aM+b) \sqrt{\theta(h) \left(1 + \frac{\gamma-1}{2} M^2\right)} \tag{27}$$

where a and b are some constant specific to a particular propulsor and $\theta(h) = \frac{T(h)}{T_{SL}}$ is the temperature ratio where $T(h)$ is the temperature at an altitude.

The maximum thrust is corrected for the Mach number and altitude according to

$$T(M,h) = (dM+e) \delta(h) \left(1 + \frac{\gamma-1}{2} M^2\right)^{\frac{\gamma}{\gamma-1}} \tag{28}$$

where d and e are some constants and $\delta(h) = \frac{P(h)}{P_{SL}}$ is the pressure ratio where $P(h)$ is the pressure at an altitude.

The singular arc optimal control dictates that the minimum-fuel climb trajectory from climb-out to cruise altitude is in accordance with the trajectory as shown in Fig. 26 [36]. The trajectory can be comprised of multiple segments but only three are illustrated. The first segment is the climb-out segment along which the aircraft accelerates and climbs at a maximum lift coefficient and maximum thrust until it intersects the singular arc segment which is described by Eq. (25) that takes into account the aircraft performance parameters. Along the singular arc segment, the aircraft lift coefficient is continuously reduced in a controlled manner to maintain the correct relationship between the airspeed and altitude while the total maximum thrust varies accordingly with the airspeed and altitude. The aircraft continues to climb along the singular arc segment until it intersects the final segment when it nearly achieves the desired cruise altitude and airspeed. Then the aircraft departs from the singular arc segment and follows the final segment until it reaches the desired airspeed and altitude. Using the singular arc minimum-fuel optimal climb, the baseline aircraft burns about 3,100 pounds of fuel during climb. The continuous descent may be approximated as an optimal climb with a negative excess thrust.

A cruise range analysis is conducted for both single-generator and dual-generator distributed propulsion aircraft. Since the aerodynamic characteristics are similar between the two configurations, the results of the dual-generator configuration are not shown. The cruise range analysis is shown for the single-generator distributed propulsion aircraft with the stiff wings and flexible wing in Figs. 27 and 28, respectively, as a function of the cruise altitude. Two types of cruise are considered, cruise at constant Mach number and altitude, and cruise at constant Mach number and angle of attack while the altitude is varied to achieve a maximum L/D. The cruise Mach number is Mach 0.8. Various thrust distributions are considered. Figure 27 reveals that the aeroelastic wing shaping control concept for the single-generator distributed propulsion aircraft with the stiff wings achieves a better cruise range than the baseline aircraft. The maximum range is achieved with a uniform thrust at about 33,000 ft for 50,000 lbs of fuel.

Figure 28 reveals that the increased wing flexibility has a significant effect on the cruise range. Overall, there is a small net reduction in the maximum cruise range as compared to the stiff wings. This is due to the non-optimal jig-shape twist for the flexible wings being the same as the design jig-shape twist for the stiff wings. Nonetheless, with a suitable thrust distribution, this reduction in the cruise range can be mostly recovered. Increasing thrust of the outboard propulsors generally causes a reduction in the cruise range. The maximum range is achieved at about 32,000 ft by increasing thrust of the two inboard propulsors by 50% of the average uniform thrust while reducing thrust of the two outboard propulsors by the same amount.
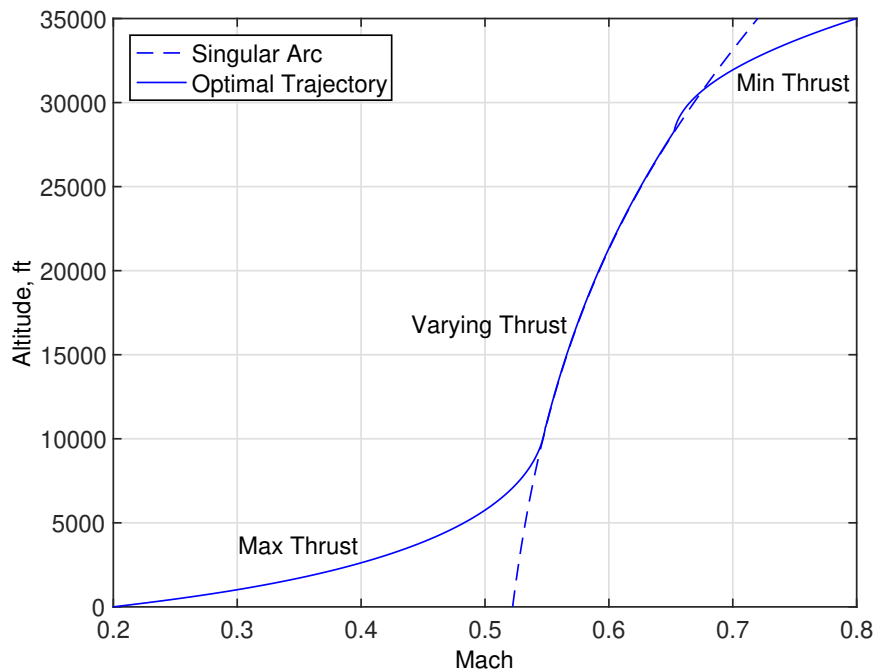

Figure 26: Singular Arc Minimum-Fuel Optimal Climb Trajectory

Figures 29 and 30 show the cruise ranges of the single-generator distributed propulsion aircraft with the stiff wings and flexible wings, respectively, as a function of fuel consumption for the maximum L/D cruise. For the stiff wings, there are small variations in the cruise range among different thrust distributions. For the flexible wings, the thrust distribution with 50% increase in thrust of the inboard propulsors and 50% decrease in thrust of the outboard propulsors produces the highest cruise

range. On the other hand, the thrust distribution with 75% increase in thrust of the outboard propulsors and 75% decrease in thrust of the inboard propulsors is the least efficient for cruise.
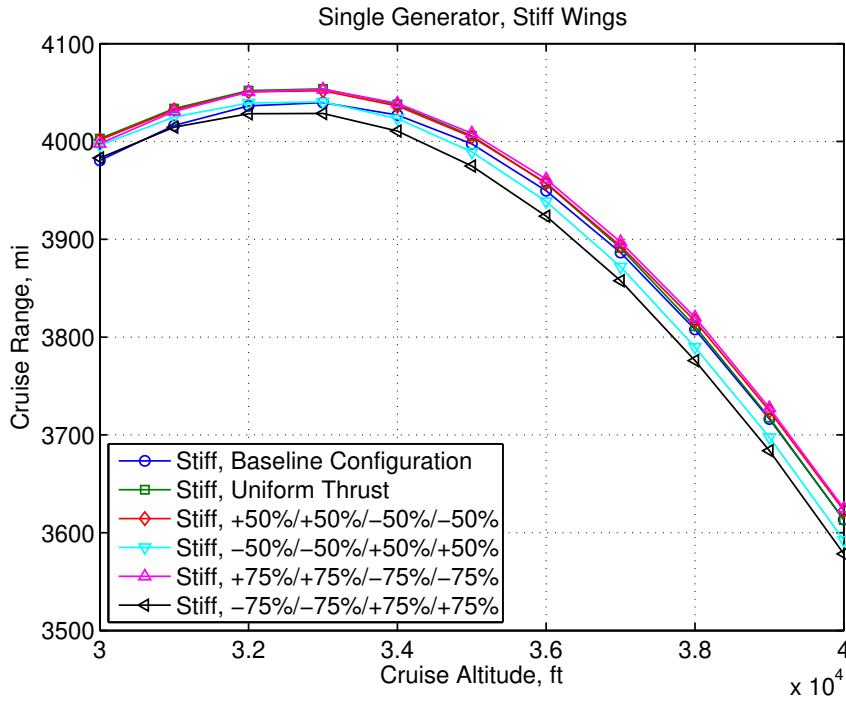

Figure 27: Maximum Range of Single-Generator Distributed Propulsion Aircraft with Stiff Wings for 50,000 lb Fuel
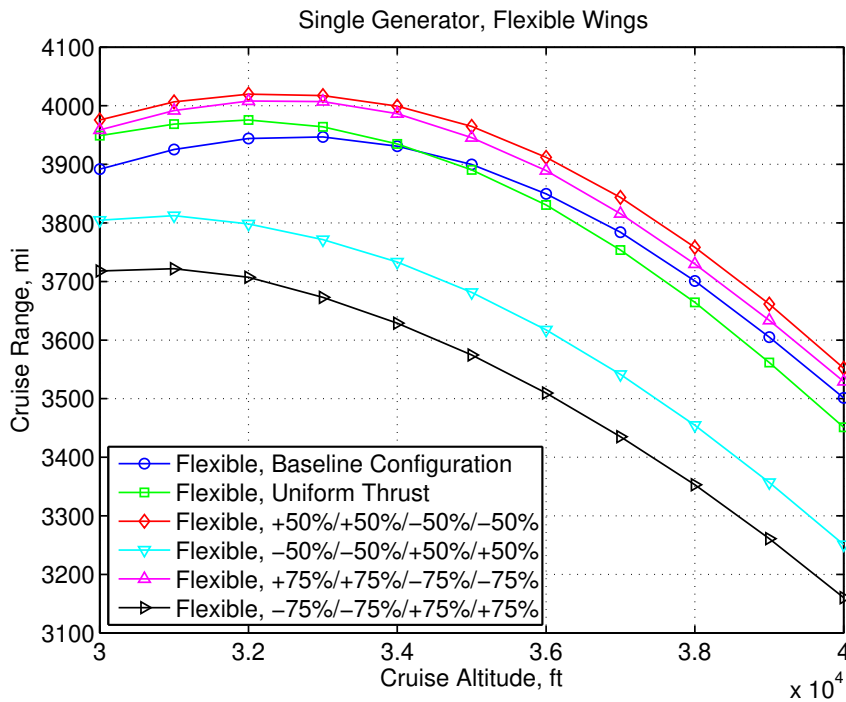

Figure 28: Maximum Range of Single-Generator Distributed Propulsion Aircraft with Flexible Wings for 50,000 lb Fuel
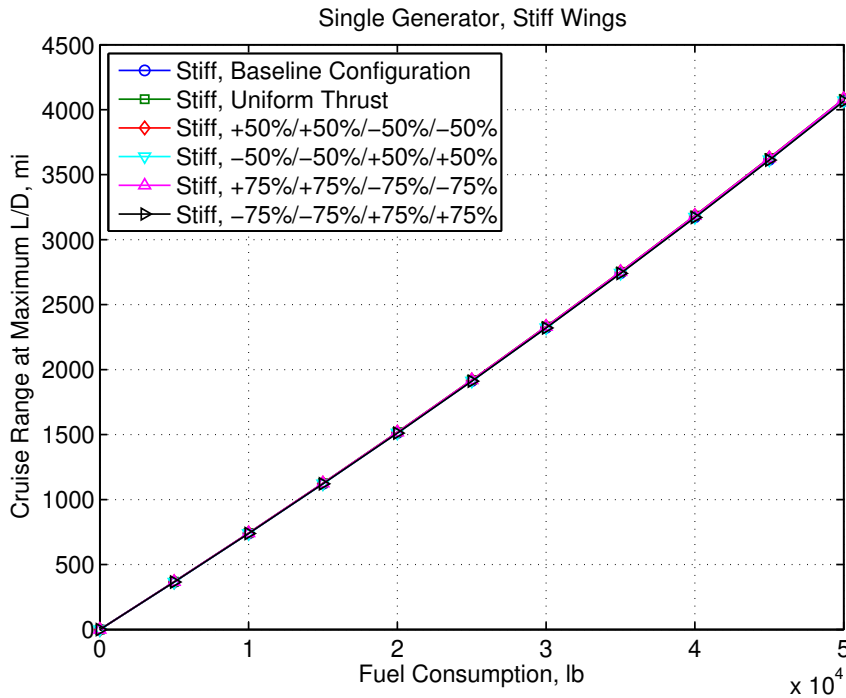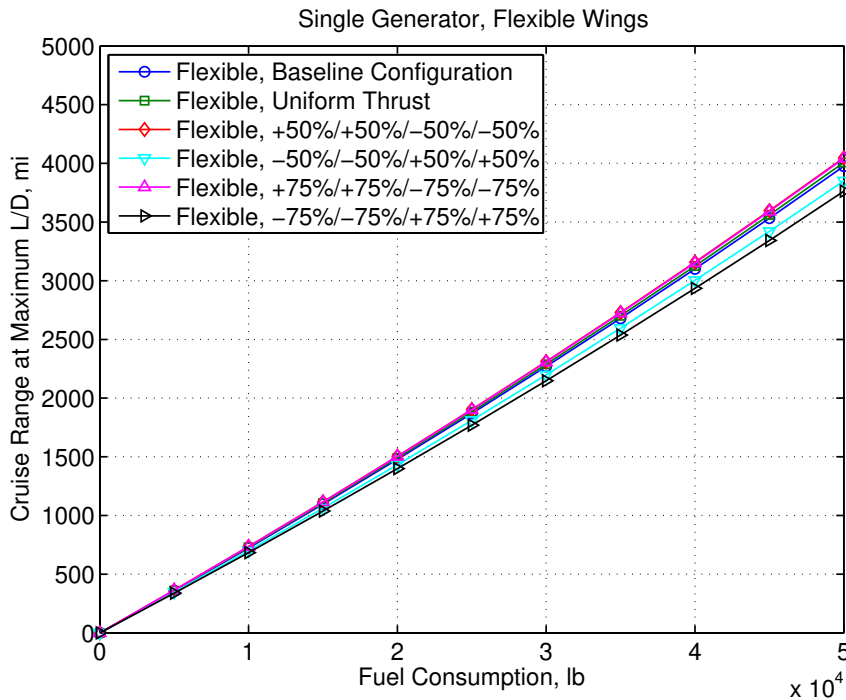
Figure 29: Maximum Range of Single-Generator Distributed Propulsion Aircraft with Stiff Wings for 50,000 lb Fuel

Figure 30: Maximum Range of Single-Generator Distributed Propulsion Aircraft with Flexible Wings for 50,000 lb Fuel

Figures 31 and 32 show the aircraft weight variation along the maximum L/D cruise trajectories for the single-generator distributed propulsion aircraft with the stiff wings and flexible wings, respectively. By maintaining a maximum L/D, the cruise altitude increases. This is known as a climb cruise. In particular, the climb cruise altitude as a function of the aircraft weight for the single-generator distributed propulsion aircraft is shown. It may be seen from comparing Fig. 31 to Fig. 32 that distributing thrust along a flexible wing enables a wider range of optimal climb cruise trajectories. More particularly, it can be seen that by

changing the thrust distribution along the flexible wings, an optimally efficient cruise altitude over a substantially greater cruise range can be selected, as compared to the stiff wings.
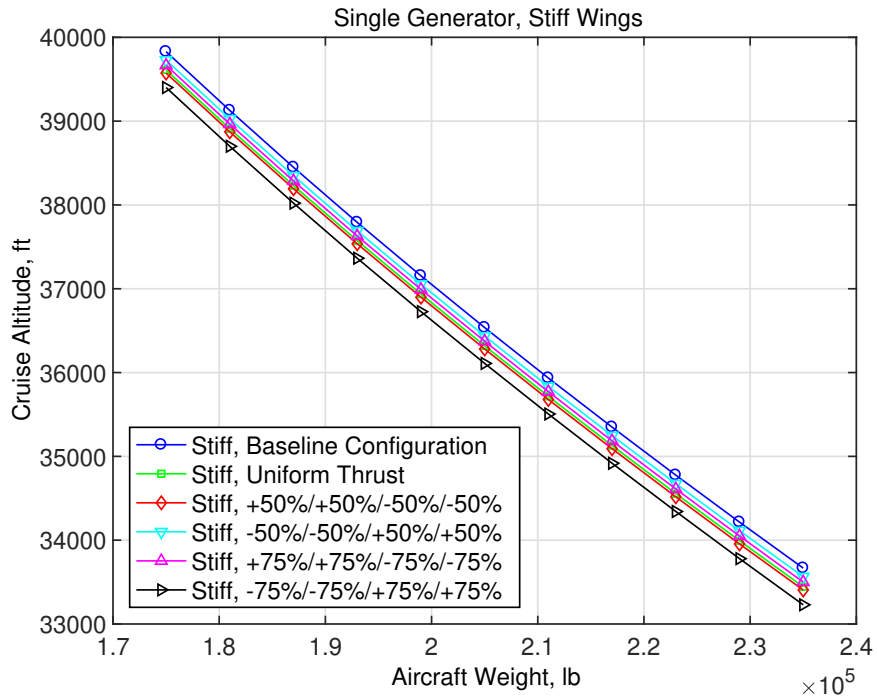

Figure 31: Constant Maximum L/D Cruise Altitude for Single-Generator Distributed Propulsion Aircraft with Stiff Wings
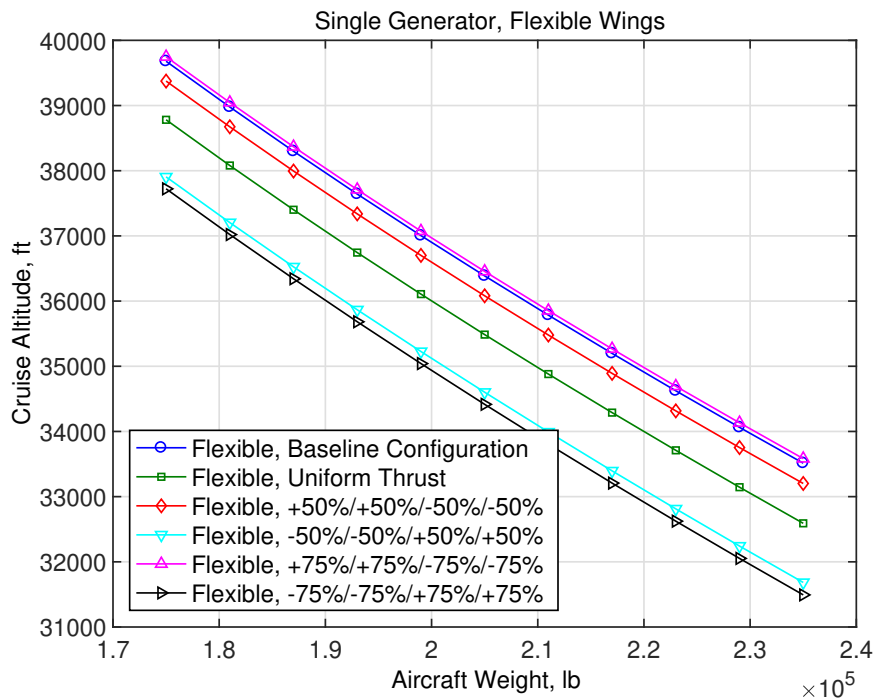

Figure 32: Constant Maximum L/D Cruise Altitude for Single-Generator Distributed Propulsion Aircraft with Flexible Wings

The improvement in the cruise range is summarized in Fig. 33 for the single-generator and dual-generator distributed propulsion aircraft with the stiff wings and the flexible wings and with various thrust distributions. As can be seen, the cruise

range is improved by about 2% with the flexible wings. This directly translates into about the same percentage reduction in the fuel consumption for the same cruise range. Increasing thrust of the inboard propulsors generally results in an improved L/D. On the other hand, the effect of the wing flexibility exacerbates the L/D benefit if more thrust is applied to the outboard propulsors than the inboard propulsors. The single-generator distributed propulsion aircraft has a slightly better improvement in the cruise range than the dual-generator distributed propulsion aircraft.

It should be noted that the results are based on a preliminary conceptual coupled aero-propulsive-elastic analysis. The exact benefit of distributed propulsion aircraft can depend on many important factors. These results would need to be further refined using high-fidelity CFD and better propulsion and weight models. Also, the configurations in the study are pre-selected without any consideration for a multidisciplinary design optimization. Opportunities for further improvement therefore exist and can be afforded by a multidisciplinary design optimization that involves various design parameters and permutations including the number and types of propulsors, the chordwise and spanwise placement location, wing flexibility, fan size, and wing shape. Also in the analysis above, the weight reduction benefit of the flexible wings is not accounted for when in fact there would be a weight credit given for a more flexible but lighter wing structure.
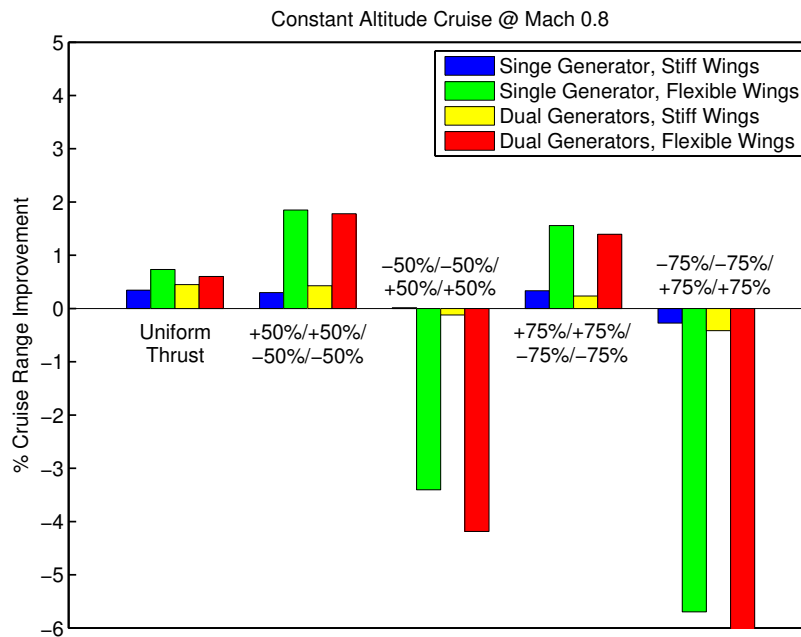

Figure 33: Cruise Range Improvement over Baseline for Various Distributed Propulsion Aircraft with Wing Shaping Concept

3.4 Flutter Analysis

As the propulsors move toward the wing tip, the generalized mass of the wing structure increases. A flutter analysis is performed to address the potential flutter issue as the propulsors affect the mass distributions and, thus, modal shapes. For the baseline GTM, the turbofan engines weigh 11,500 lbs each. With the single-generator distributed propulsion aircraft, the generators weigh 5,626 lbs each. To reduce the generalized mass, the generators are moved further inboard from the wing stations of the turbofan engines for the baseline GTM. The propulsors weigh 1,840 lbs each. The total weight of the propulsors plus the generator is 12,986 lbs.

A preliminary flutter analysis is performed to assess the effect of mass placement along the wing span for the single-generator distributed propulsion aircraft [33]. Figures 34-39 are the results of the flutter analysis presented in terms of the aeroelastic frequencies and structural damping for both symmetric and anti-symmetric modes as a function of the equivalent airspeed. For the flutter analysis, a structural damping of 1% modeled as an equivalent viscous damping of 0.5%.

The flutter speed of the baseline GTM occurs at an equivalent airspeed of 508.77 knots, corresponding to the 1st anti-symmetric mode at a flutter frequency of 19.34 rad/sec. This equivalent airspeed corresponds to Mach 0.7667 at sea level.

For the single-generator distributed propulsion aircraft with the stiff wings, the flutter speed occurs at an equivalent airspeed of 631.35 knots, corresponding to the 1st anti-symmetric mode at a flutter frequency of 15.13 rad/sec. It is interesting to note that the flutter speed of the distributed propulsion aircraft with the stiff wings is higher than that for the baseline GTM even

though the natural frequencies are lower as a result of the increased generalized mass of the distributed propulsion system. This is likely due to the changes in the frequency separation between the bending modes and torsion modes in a favorable way for the distributed propulsion aircraft as compared to the baseline GTM.
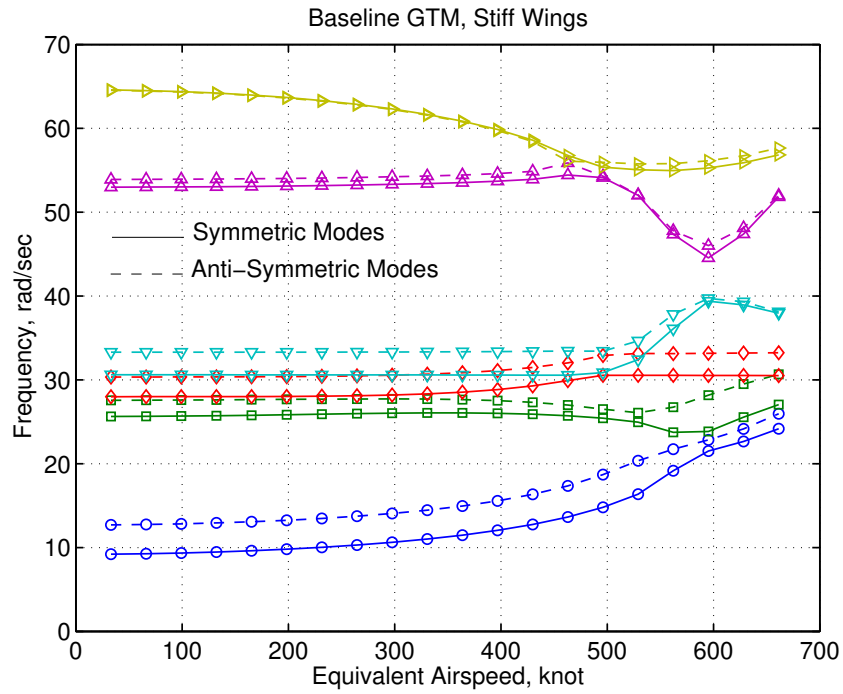

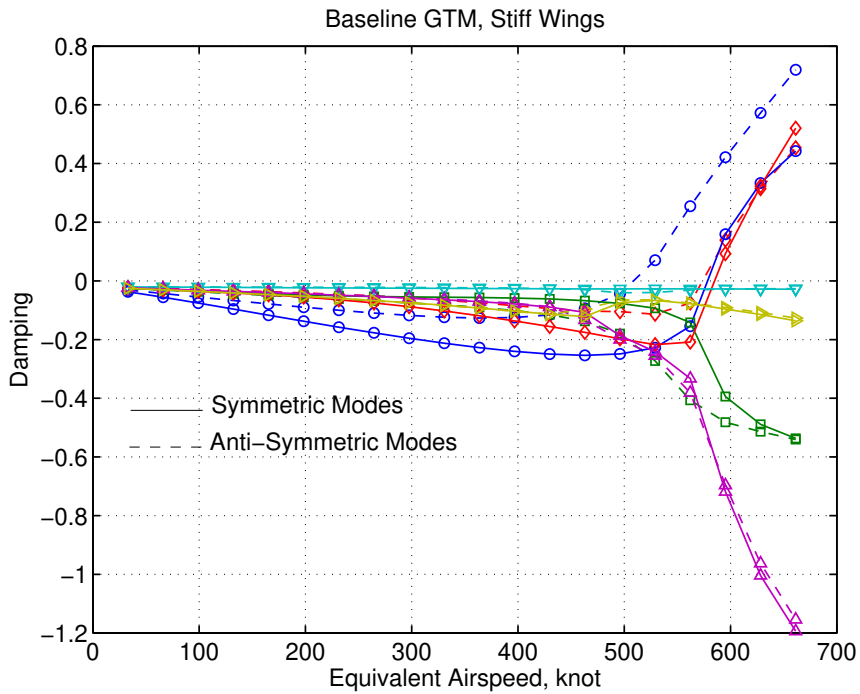Figure 34: Frequencies of Baseline GTM with Stiff Wings

Figure 35: Damping of Baseline GTM with Stiff Wings
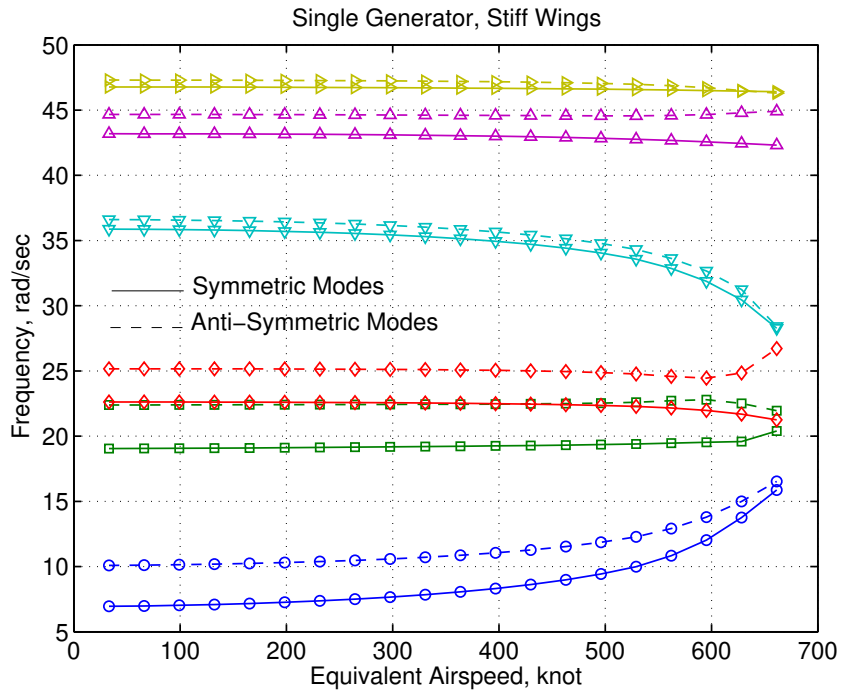
Figure 36: Frequencies of Single-Generator Distributed Propulsion Aircraft with Stiff Wings
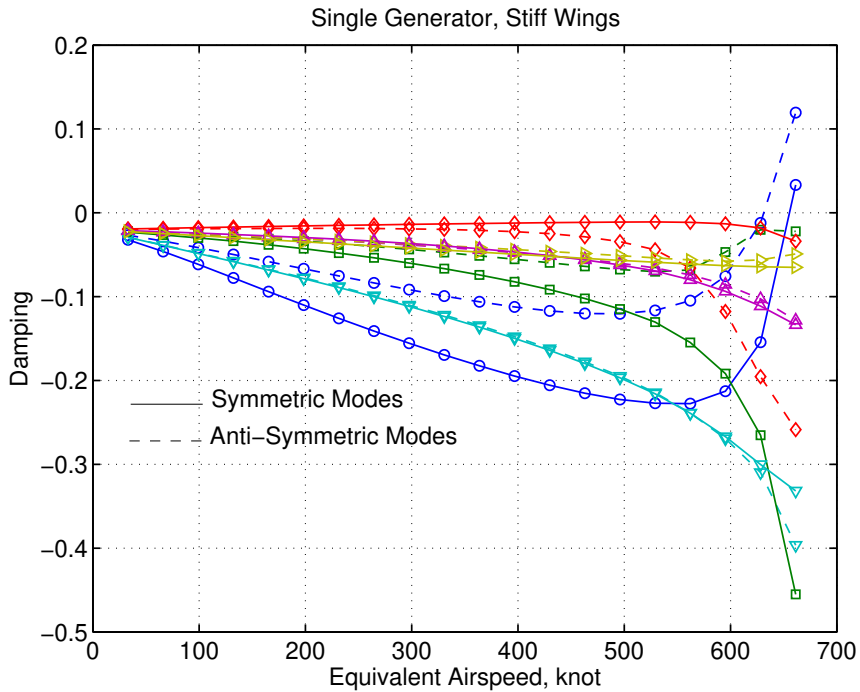

Figure 37: Damping of Single-Generator Distributed Propulsion Aircraft with Stiff Wings

For the single-generator distributed propulsion aircraft with the flexible wings, the flutter speed occurs at an equivalent airspeed of 562.80 knots, corresponding to the 1st anti-symmetric mode at a flutter frequency of 11.68 rad/sec. This flutter speed is lower than that for the stiff wings, but yet is higher than that for the baseline GTM. It should be noted that the flexible wings are with the reduced torsional stiffness while the bending stiffness is the same as that for the stiff wings. Thus, based on the preliminary flutter analysis, it appears that the single-generator distributed propulsion aircraft with the flexible wings would

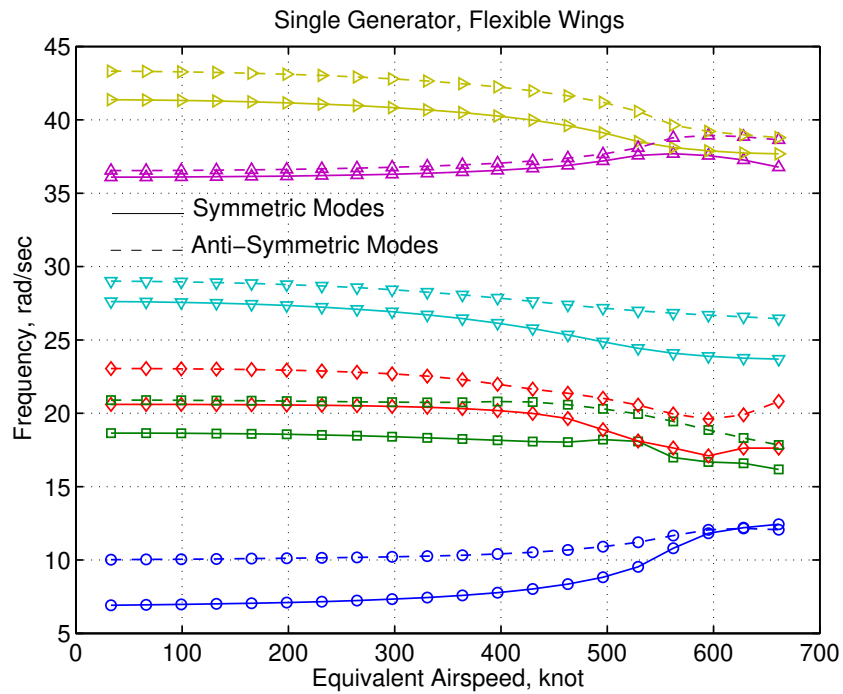be able to meet flutter clearance requirements.

Figure 38: Frequencies of Single-Generator Distributed Propulsion Aircraft with Flexible Wings
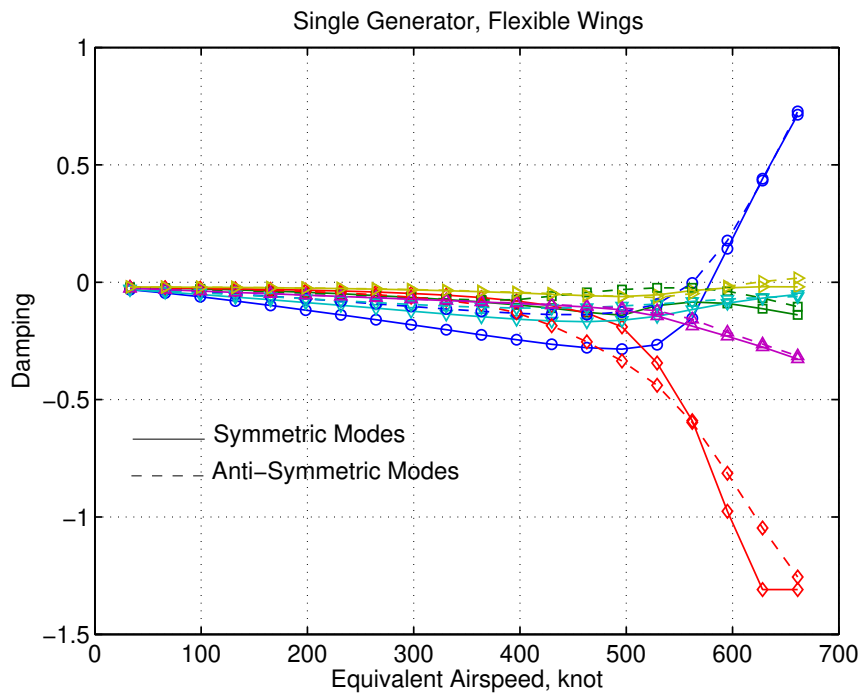

Figure 39: Damping of Single-Generator Distributed Propulsion Aircraft with Flexible Wings

This flutter analysis serves to illustrate the multidisciplinary design aspect of distributed propulsion aircraft. Such vehicle configurations will require a multidisciplinary design optimization approach that can provide a trade-off between many important factors such as aircraft performance and flutter constraints.

3.5 Flight Control Consideration for Distributed Propulsion Aircraft

The vertical tail provides the directional stability to an aircraft. It is usually sized for the required engine-out condition at the maximum take-off thrust. In conjunction, the rudder is designed to impart a yawing moment for directional control and yaw stability augmentation. In an event of power loss to one of the conventional gas turbine engines, the rudder can be deployed to counteract the yawing moment due to the asymmetric thrust.
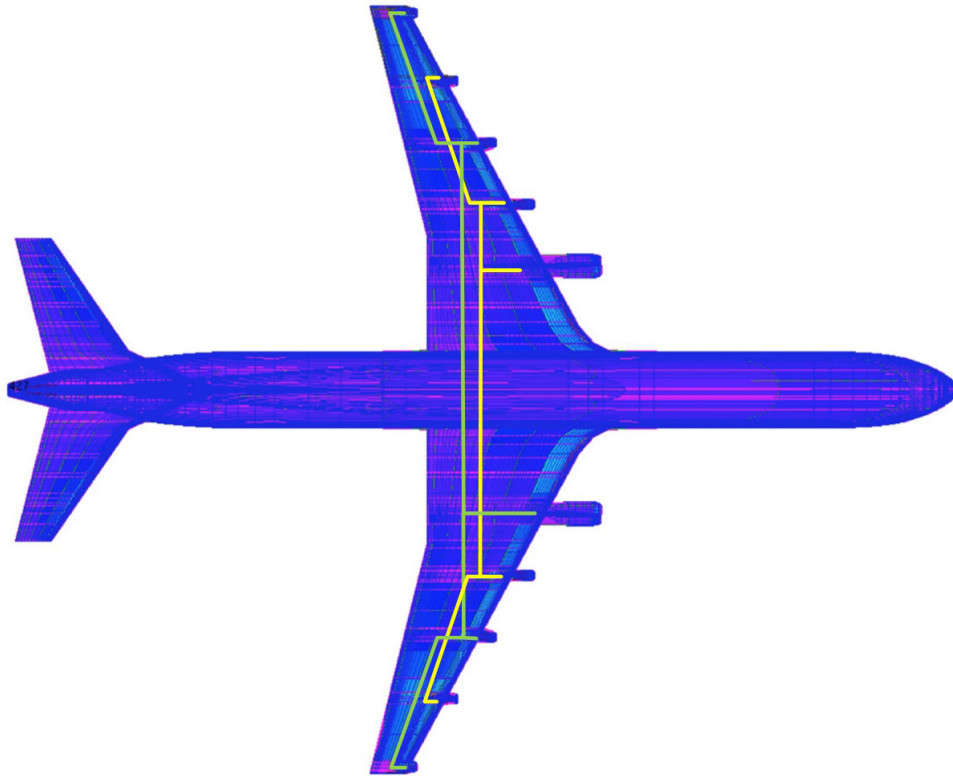

Figure 40: Power Distribution to Minimize Engine-Out Yawing Moment

The gas turbine generators generate the power necessary to drive the propulsors. Electrical distribution systems can designed in such a way that could minimize the engine-out yawing moment. One such power distribution is shown in Fig. 40 whereby each of the generators drives two pairs of propulsors placed symmetrically on the wings. This may be feasible if the electrical line loss in the power distribution systems is not significant, and or if such power distribution arrangements can be accommodated conveniently in an airframe design. Under these assumptions, no yawing moment would be created in an event of power loss to either generator. This is a highly idealized scenario. In practice, there will likely be an engine-out yawing moment, the magnitude of which could be tailored by advantageous power distribution schemes. In any event, the vertical tail can be reduced in size to provide only the yaw control and stability augmentation as needed. As the vertical tail is reduced, the potential aircraft weight reduction benefit could be realized.

Figure 41 shows the weight reduction due to the vertical tail of the GTM as a function of the reduced vertical tail span. On the other hand, the frequency and damping of the Dutch-roll mode for the GTM also decrease accordingly as shown in Figs. 42 and 43. It can be seen that the damping of the dutch-roll mode is relatively insensitive to vertical tail size up to about 75% span reduction. In order to maintain desired pilot handling qualities, yaw damping augmentation is usually implemented in the rudder control system to increase the Dutch-roll damping to a desired level. Thus, the rudder control system would need to be redesigned with increased actuator power to meet the Dutch-roll damping requirement. Thus, distributed propulsion provides an opportunity to optimize the vertical tail size and the rudder actuator system for weight reduction to further improve fuel efficiency.

Another benefit of distributed propulsion is the ability to deploy differential thrust for yaw control. Flight-propulsion control using differential thrust for yaw control was investigated in the past as a backup flight control system [37] which was inspired by the United Airlines accident at Sioux City, Iowa [38]. Figure 44 illustrates the differential thrust yaw control. The differential thrust can be generated by either reducing the thrust level of the propulsors on one wing or increasing the thrust level of the propulsors on the other wing. The thrust distribution on one wing can either be uniform as shown in Fig. 44 or vary along the wing span. A flight control system can be designed to automatically generate suitable differential thrust commands to the

individual propulsors to generate a necessary yawing moment to yaw the aircraft.
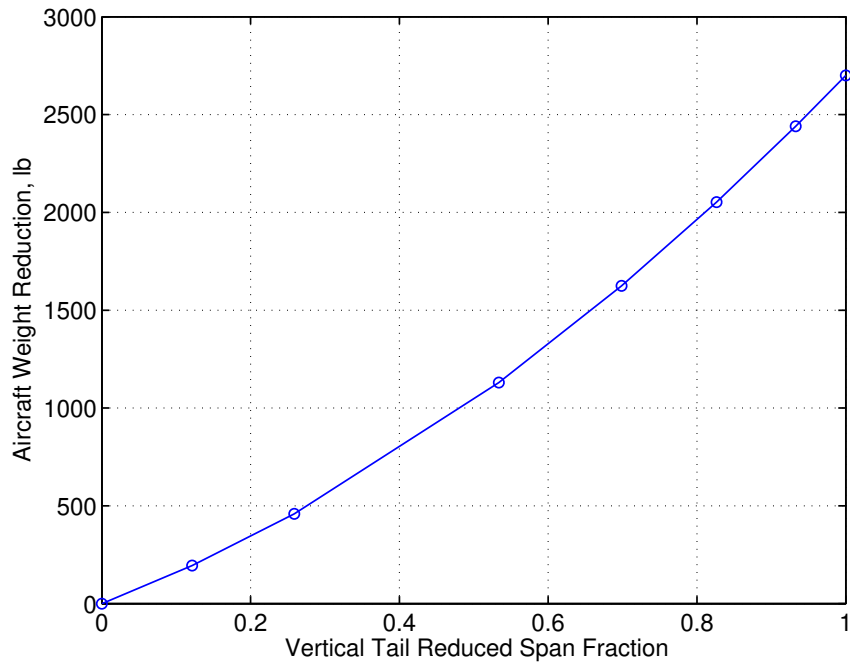

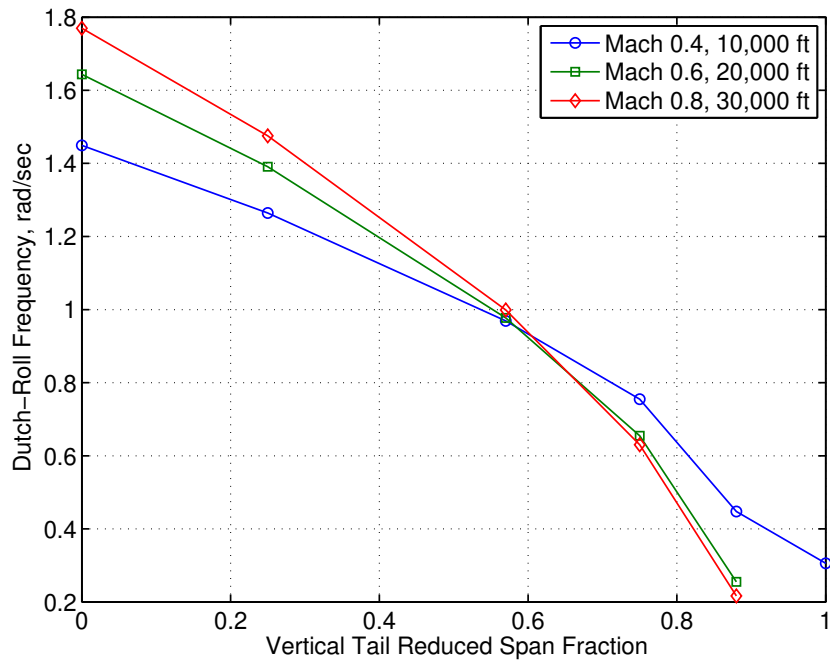Figure 41: Aircraft Weight Reduction as a Function of Vertical Tail Reduced Span Fraction

Figure 42: Frequency of Dutch-Roll Mode of the GTM as a Function of Vertical Tail Reduced Span Fraction
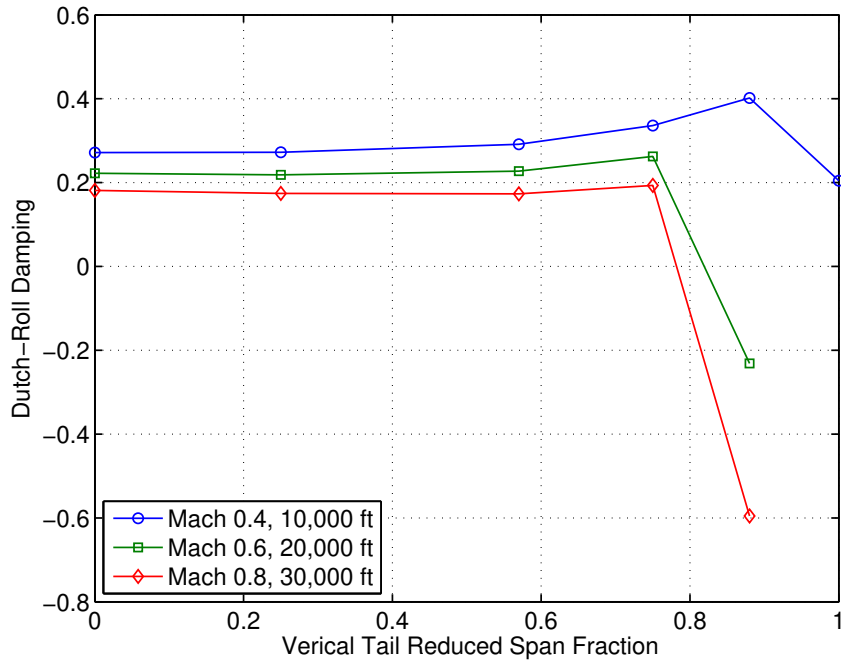
Figure 43: Frequency of Dutch-Roll Mode of the GTM as a Function of Vertical Tail Reduced Span Fraction

Figure 44: Differential Thrust Control
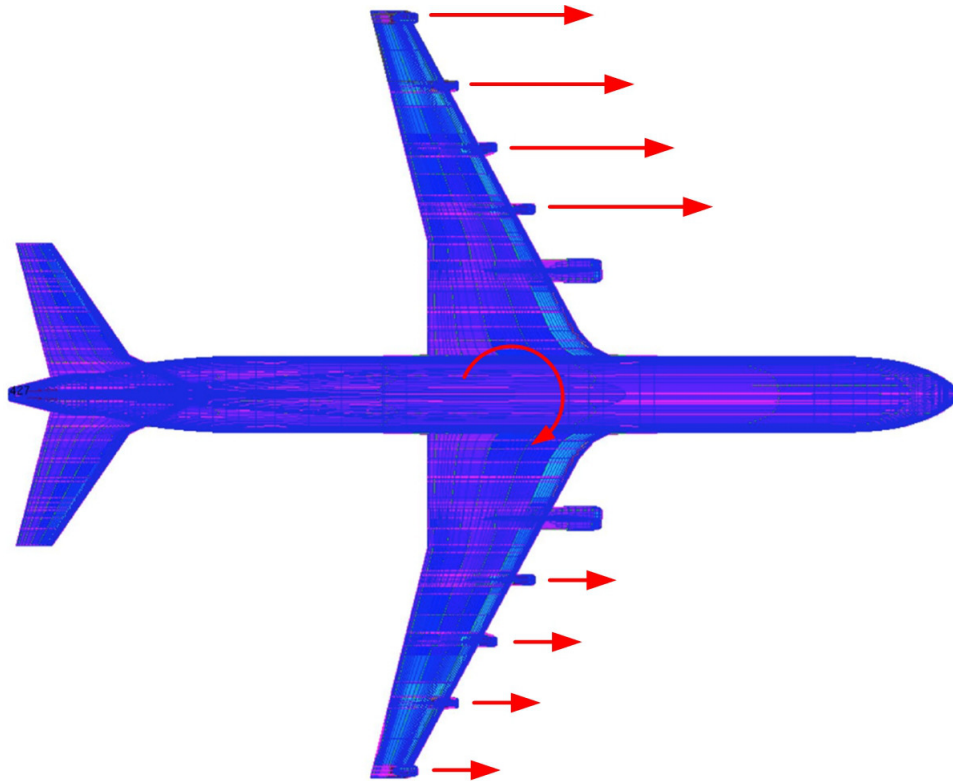
With reference to Fig. 45, the differential thrust forces create unequal lift forces acting on the aircraft wings. The thrust forces create nose-up pitching moments that twist the wing airfoil section nose-up in the direction of increasing the angle of attack. Thus, the thrust-induced lift forces are generated due to the thrust forces produced by the propulsors. Referring to Fig.

44, the thrust forces created by the propulsors on the left wing are greater than the thrust forces created by the propulsors on the right wing. Thus, the thrust-induced lift forces on the left wing are greater than those on the right wing. As a result, a rolling moment is produced from the unequal thrust-induced lift forces to roll the aircraft to the right with the left wing up. The yawing moment created by the differential thrust causes the aircraft to yaw to the right, and thus is also accompanied by a favorable rolling moment to make a coordinated turn in which the aircraft rolls into the direction of the turn as it yaws. This favorable rolling moment thus can allow a coordinated turn to be controlled using only differential thrust without a rudder input. In contrast, a coordinated turn maneuver in a conventional aircraft requires both rudder and aileron inputs simultaneously. Furthermore, when rolling using ailerons, an adverse yaw due to the incremental drag forces is produced that tends to yaw the aircraft away from the turn, thus requiring an extra rudder input to overcome the adverse yaw. It can be seen that differential thrust yaw control using distributed propulsion affords an advantage over a conventional flight control for coordinated turn maneuvers.

Pure roll control is also possible with the deployment of differential thrust using distributed propulsion. A rudder input can be programmed automatically in a flight control system to cancel out the yawing moment produced by the differential thrust, while the rolling moment due to the thrust-induced lift enables the aircraft to perform pure roll. In contrast, a conventional aircraft performs pure roll by the application of an aileron input and a rudder input to cancel out the adverse yaw. Pure yaw control is important in situations of landing in cross wind. A conventional aircraft performs pure yaw by the application of a rudder input and a small aileron input to maintain wing level due to the roll-yaw coupling. Pure yaw control is possible with differential thrust using distributed propulsion. An aileron input is programmed in a flight control system to cancel out the rolling moment generated by thrust-induced lift forces.
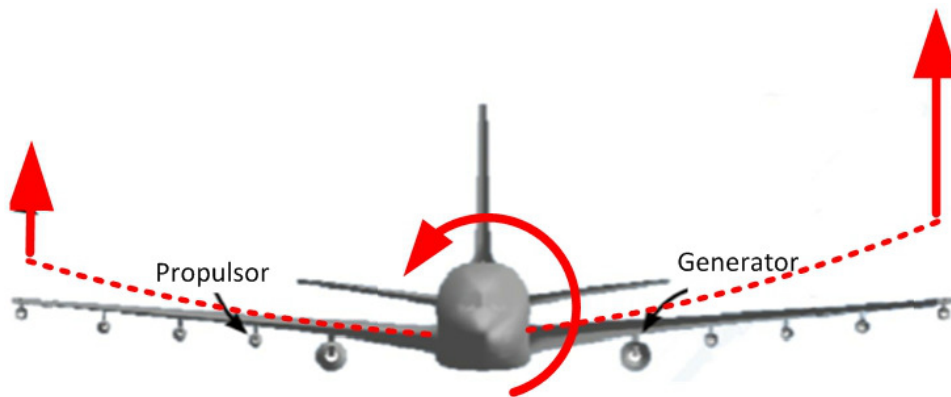

Figure 45: Thrust-Induced Rolling Moment and Proverse Yaw

Figure 46 illustrates a flight control system for using differential thrust to control roll and yaw motions of distributed propulsion aircraft. The flight control system receives a pilot command to initiate a coordinated turn, a pure yaw, or a pure roll. A control mode selection selects a desired controller to achieve a coordinated turn command, yaw command, or roll command. Each of the control modes is accomplished as follows:

- The coordinated turn command is used as the input into a coordinated turn controller to generate the necessary command of differential thrust for distributed propulsion. The output differential thrust causes the aircraft to change its motion. The response of the aircraft is then fed back into the coordinated turn controller to zero out the error to achieve the desired coordinated turn.

- The yaw command is used as the input into a yaw controller. Two command signals are generated by the yaw controller: a differential thrust command for distributed propulsion and an aileron command for the aileron. The differential thrust causes the aircraft to yaw while the aileron deflection keeps the aircraft wing level by canceling out the thrust-induced rolling moment. The response of the aircraft is fed back into the yaw controller to achieve the desired yaw motion.

- The roll command is used as the input into the roll controller. A differential thrust command and an aileron command are generated by the roll controller. These commands are received by distributed propulsion and the aileron which generate the aileron deflection to cause the aircraft to roll while the differential thrust cancels out the adverse yaw due to the aileron deflection. The response of the aircraft is fed back into the roll controller to achieve the desired roll motion. Alternatively, the roll command can also be achieved by using a differential thrust command to generate a thrust-induced rolling moment and a rudder command to cancel out the proverse yaw.
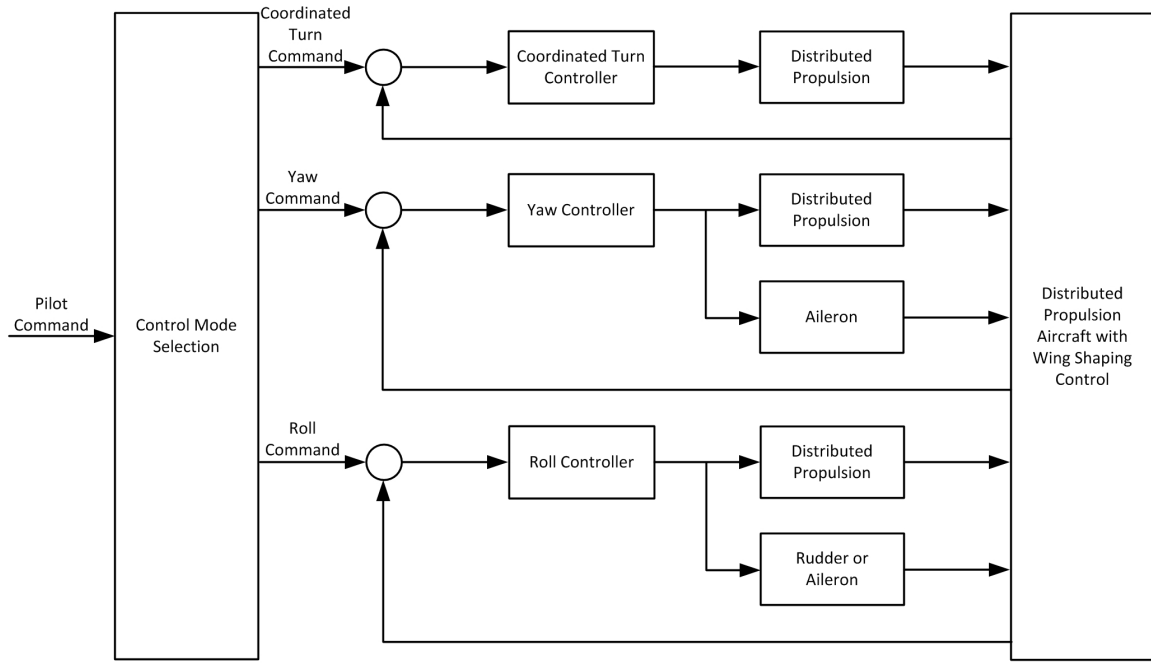
Figure 46: Differential Thrust Flight Control System

The flight controller is designed using the following equation that represents the lateral-directional dynamics of the aircraft.

$$
\begin{bmatrix} \dot{\beta} \\ \dot{p} \\ \dot{r} \\ \dot{\phi} \\ \dot{\psi} \end{bmatrix} = \begin{bmatrix} \frac{Y_\beta}{\bar{u}} & \frac{Y_p}{\bar{u}}+\bar{\alpha} & \frac{Y_r}{\bar{u}}-1 & \frac{g}{\bar{u}} & 0 \\ L_\beta & L_p & L_r & 0 & 0 \\ N_\beta & N_p & N_r & 0 & 0 \\ 0 & 1 & 0 & 0 & 0 \\ 0 & 0 & 1 & 0 & 0 \end{bmatrix} \begin{bmatrix} \beta \\ p \\ r \\ \phi \\ \psi \end{bmatrix} + \begin{bmatrix} \frac{Y_{\delta_a}}{\bar{u}} & \frac{Y_{\delta_r}}{\bar{u}} & \frac{Y_{\delta_{T_L}}}{\bar{u}} & \frac{Y_{\delta_{T_R}}}{\bar{u}} \\ L_{\delta_a} & L_{\delta_r} & L_{\delta_{T_L}} & L_{\delta_{T_R}} \\ N_{\delta_a} & N_{\delta_r} & N_{\delta_{T_L}} & N_{\delta_{T_R}} \\ 0 & 0 & 0 & 0 \\ 0 & 0 & 0 & 0 \end{bmatrix} \begin{bmatrix} \delta_a \\ \delta_r \\ \delta_{T_L} \\ \delta_{T_R} \end{bmatrix} \tag{29}
$$

where β is the sideslip angle, p is the roll rate, r is the pitch rate, ϕ is the bank angle, ψ is the heading angle, Y is the dimensional side force derivative, L is the dimensional rolling moment derivative, N is the dimensional yawing moment derivative, δ_a is the aileron deflection, δ_r is the rudder deflection, and δ_{T_L} and δ_{T_R} are the vectors of the incremental thrust forces on the left wing and right wing, respectively.

Note that the thrust-induced rolling moment terms $L_{\delta_{T_R}}$ and $L_{\delta_{T_R}}$ are due to the thrust-induced lift, which is created by the aero-propulsive-elastic effect of the flexible wings.

When differential thrust is used in a flight control system, the thrust dynamics must be considered. In general, aircraft gas turbine engines are too slow for use in a flight control system. The transport delay due to the fluid motion as it passes through a gas turbine engine prevents using differential thrust control for yaw stability augmentation. Therefore, the vertical tail and rudder are needed for yaw stability augmentation. Differential thrust can still be used for heading angle command. A typical thrust response to the throttle command is shown in Fig. 47 based on a simplified engine dynamic model C-MAPSS40k developed by NASA Glenn Research Center for a 40,000-lb thrust gas turbine engine class that powers the GTM [39]. The model is based on actual flight test data collected at various flight conditions. The model generates the engine thrust response as a function of the throttle resolver angle (TRA) at a given flight condition specified by the Mach number and altitude. Even with simplification, the nonlinear engine dynamic model is still quite complex. This nonlinear engine dynamic model is further simplified as a time-delayed second-order model as [40]

$$
\ddot{T}+2\zeta\omega\dot{T}+\omega^2 T = \omega^2 T_c\left(t-t_d\right) \tag{30}
$$

where ζ and ω are the damping ratio and bandwidth frequency of the closed-loop engine dynamics, and T_c is the engine thrust command which is prescribed by an engine TRA.

The engine time delay t_d is generally dependent on the initial thrust level according to an inverse relationship. That is, the larger the initial thrust level is that an engine operates at, the smaller the engine time delay is. The time constant of the engine response dictates how fast the engine thrust rises. The time constant may be defined as

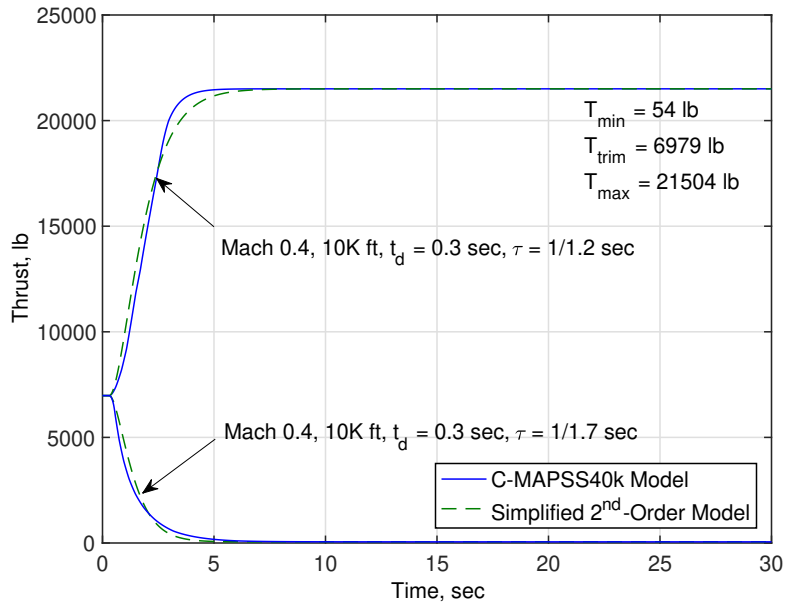$$
\tau = \frac{1}{\omega} \tag{31}
$$

Figure 47: Thrust Response to Thrust Command for a 40,000-lb Gas Turbine Engine Class
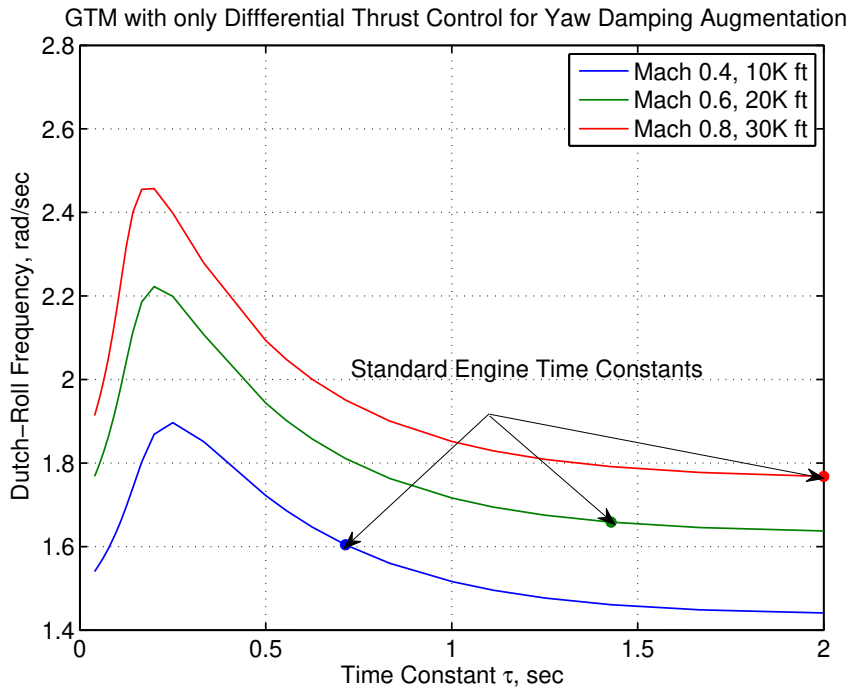

Figure 48: Dutch-Roll Frequency of GTM Using Differential Thrust Control without Rudder

The transport delay can affect the ability for yaw stability augmentation using only differential thrust control. Figures 48 and 49 show the frequency and damping of the Dutch-roll mode of the GTM as a function of the transport delay for a typical 40,000-lb engine class [40]. As the transport delay increases, the frequency and damping of the Dutch-roll mode generally decrease. With small-size propulsors, the transport delay will be smaller than the typical transport delay for a gas turbine engine. Thus, the possibility of yaw stability augmentation may exist with distributed propulsion. Figure 49 shows that the closed-loop Dutch-roll damping with differential thrust control could only be as much as 0.5 of the critical damping ratio if the transport delay is kept below 0.1 second. In addition, the frequency bandwidth of the propulsors must be sufficiently large in

order to achieve a desired yaw damping augmentation. As a rough estimate, this frequency bandwidth should be about an order of magnitude higher than the Dutch-roll frequency or about 20 rad/sec which corresponds to a time constant of 0.05 sec. Then, in theory, the rudder can be reduced in size to further augment the Dutch-roll damping to achieve a desired value.
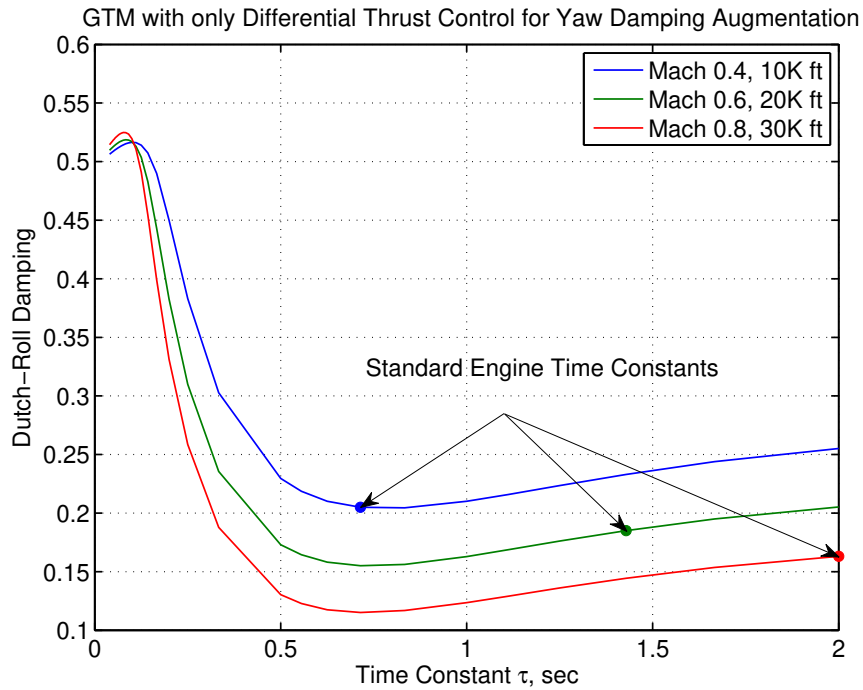

Figure 49: Dutch-Roll Damping of GTM Using Differential Thrust Control without Rudder

4 Conclusions

This study presents an aeroelastic wing shaping control concept for distributed propulsion aircraft. By leveraging the thrust-induced lift effect resulting from wing aeroelasticity, it can be shown that distributed propulsion could be used to increase the aerodynamic efficiency. Preliminary aerodynamic analysis and performance analysis are carried out to assess the merit of this concept based on the NASA Generic Transport Model. An improvement of about 2% could be realized with the distributed propulsion aircraft when the wing torsional stiffness is reduced by a factor of 2. This improvement is associated with a thrust distribution that has 50% more thrust on the inboard propulsors and 50% less thrust on the outboard propulsors as compared to the uniform thrust distribution. The single-generator configuration has a slightly higher cruise range improvement than the dual-generator configuration.

A flutter consideration is taken into account to address the potential frequency reduction as the propulsors are placed toward the wing tip. A preliminary flutter analysis shows that the single-generator distributed propulsion aircraft would be able to meet flutter clearance requirements with either the baseline stiff wings or the flexible wings. The increase in the flutter speed is perhaps due to a favorable change in the frequency separation between the bending and torsion modes.

Flight control considerations are addressed for distributed propulsion aircraft in concert with aeroelastic wing shaping control. With the potential flexibility in the power distribution arrangement, it may be possible to reduce to effect of the engine-out yawing moment when one of the generators is disabled. This could result in a potential weight reduction benefit due to a reduced vertical tail size. Yaw control using differential thrust creates a proverse yaw benefit due to the thrust-induced rolling moment. Pure roll control may be possible with distributed propulsion aircraft by also leveraging the thrust-induced rolling moment. Consideration of the yaw damping augmentation can be made possible by including differential thrust control using distributed propulsion. The issue of slow transport time delay which currently limits the use of conventional gas turbine engines for differential thrust control for yaw damping augmentation may be ameliorated with distributed propulsion as afforded by smaller propulsors which generally would have a smaller time transport delay. Nonetheless, using distributed propulsion for yaw damping augmentation in conjunction with the rudder may be a challenging proposition.

Acknowledgment

References

[1] Kim, H. D., "Distributed Propulsion Vehicles," Proceedings of 27th International Congress of the Aeronautical Sciences, Curran Associates, Inc., Red Hook, NY, September 2010.

[2] Felder, J., Kim H., and Brown, G. "Turboelectric Distributed Propulsion Engine Cycle Analysis for Hybrid-Wing-Body Aircraft," 47th AIAA Aerospace Sciences Meeting, AIAA-2009-1132, January 2009. DOI: 10.2514/6.2009-1132

[3] Gibson, A., Hall, D., Waters, M., Masson, P., Schiltgen, B., Foster, T., and Keith, J., "The Potential and Challenge of TurboElectric Propulsion for Subsonic Transport Aircraft," AIAA 2010-276, 48th AIAA Aerospace Sciences Meeting, January 2010. DOI: 10.2514/6.2010-276

[4] Uranga, A., Drela, M., Greitzer, E., Titchener, N., Lieu, M., Siu, N., Huang, A., Gatlin, G. M., and Hannon, J., "Preliminary Experimental Assessment of the Boundary Layer Ingestion Benefit for the D8 Aircraft," 52nd Aerospace Sciences Meeting, AIAA SciTech Forum, AIAA-2014-0906, January 2014. DOI: 10.2514/6.2014-0906.

[5] Moore, M., Fredericks, W., and Borer, N., "Drag Reduction Through Distributed Electric Propulsion," 14th AIAA Aviation Technology Integration, and Operations Conference, AIAA-2014-2851, June 2014. DOI: 10.2514/6.2014-2851

[6] Nguyen, N., "Active Wing Shape Control Technology for Aircraft," NASA Tech Briefs Magazine, Vol. 34, No. 4, April 2010, pp. 71.

[7] Padfield, G. D., and Lawrence, B., "The Birth of Flight Control: An Engineering Analysis of the Wright Brothers' 1902 Glider," The Aeronautical Journal, Vol. 107, No. 1078, Dec. 2003, pp. 697-713. DOI: 10.1017/S0001924000013464

[8] Pendleton, E. W., Bessette, D., Field, P. B., Miller, G. D., and Griffin, K. E., "Active Aeroelastic Wing Flight Research Program: Technical Program and Model Analytical Development," AIAA Journal of Aircraft, Vol. 37, No. 4, August 2000. DOI: 10.2514/2.2654

[9] Cheung, K., Cellucci, D., Copplestone, G., Cramer, N., Fusco, J., Jenett, B., Kim, J., Langford, A., Mazhari, A., Trinh, G., Swei, S., "Development of Mission Adaptive Digital Composite Aerostructure Technologies (MADCAT)," 17th AIAA Aviation Technology, Integration, and Operations Conference, AIAA-2017-4273, June 2017. DOI: 10.2514/6.2017-4273

[10] Cumming, S. B ., Smith, M. S., Ali, A. N., Bui, T. T., and Ellsworth, J. C., "Aerodynamic Flight-Test Results for the Adaptive Compliant Trailing Edge," AIAA Atmospheric Flight Mechanics Conference, AIAA-2016-3855, June 2016. DOI: 10.2514/6.2016-3855

[11] Vos, R. and Barrett, R. M., "Presure Adaptive Honeycomb: a Novel Concept For Morphing Aircraft Structures," 27th International Congress of the Aeronautical Sciences, September 2010.

[12] Bonnema, K. L., and Smith, S., B., "AFTI/ F-111 Mission Adaptive Wing Flight Research Program," 4th AIAA Flight Test Conference, AIAA-1988-2118, May 1988. DOI: 10.2514/6.1988-2118

[13] Gern, F. H., Inman, D. J., and Kapania, R. K., "Structural and Aeroelastic Modeling of General Planform Wings with Morphing Airfoils," AIAA Journal, Vol. 40, No. 4, April 2002. DOI: 10.2514/2.1719

[14] Nguyen, N., "Elastically Shaped Future Air Vehicle Concept," NASA Innovation Fund Project 2010 Rept., NASA Technical Report Server Report Number ARC-E-DAA-TN3743, Oct. 2010, http://ntrs.nasa.gov/archive/nasa/casi.ntrs.nasa.gov/20110023698.pdf.

[15] Nguyen, N. and Urnes, J., "Aeroelastic Modeling of Elastically Shaped Aircraft Concept via Wing Shaping Control for Drag Reduction," AIAA Atmospheric Flight Mechanics Conference, AIAA-2012-4642, August 2012. DOI: 10.2514/6.2012-4642

[16] Urnes, J., Nguyen, N., Ippolito, C., Totah, J., Trinh, K., and Ting, E., "A Mission Adaptive Variable Camber Flap Control System to Optimize High Lift and Cruise Lift to Drag Ratios of Future N+3 Transport Aircraft," 51st AIAA Aerospace Sciences Meeting, AIAA-2013-0214, January 2013. DOI: 10.2514/6.2013-214

[17] Ting, E., Chaparro, D., and Nguyen, N. T., "Aero-Structural Optimization of Variable Camber Continuous Trailing Edge Flap Configurations Using Transonic and Viscous Potential Flow Method," 35th AIAA Applied Aerodynamics Conference, AIAA-2017-4220, June 2017. DOI: 10.2514/6.2017-4220

[18] Nguyen, N., Precup, N., Urnes, J., Nelson, C., Lebofsky, S., Ting, E., and Livne, E., "Experimental Investigation of a Flexible Wing with a Variable Camber Continuous Trailing Edge Flap Design," 32nd AIAA Applied Aerodynamics, AIAA 2014-2441, June 2014. DOI: 10.2514/6.2014-2441

[19] Nguyen, N., Ting, E., Nguyen, D., and Trinh, K., "Flight Dynamic Modeling and Stability Analysis of Flexible Wing Generic Transport Aircraft," 55th AIAA/ASME/ASCE/AHS/ASC Structures, Structural Dynamics, and Materials Conference, AIAA-2014-1040, January 2014. DOI: 10.2514/6.2014-1040

[20] Fujiwara, G. E. and Nguyen, N. T., "Aerostructural Design Optimization of a Subsonic Wing with Continuous Morphing Trailing Edge," 35th AIAA Applied Aerodynamics Conference, AIAA-2017-4218, June 2017. DOI: 10.2514/6.2017-4218

[21] Ting, E., Chaparro, D., and Nguyen, N., "Development of an Integrated Nonlinear Aeroservoelastic Flight Dynamic Model of the Truss-Braced Wing Aircraft," 58th AIAA/ASME/ASCE/AHS/SC Structures, Structural Dynamics, and Materials Conference, AIAA-2017-1815, January 2017. DOI: 10.2514/6.2017-1815

[22] Reynolds, K., Nguyen, N., Ting, E., Trinh, K., Kim, H., Felder, J., Urnes, J., and Ramsey, J., "Wing Shaping Concepts Using Distributed Propulsion For Optimizing Spawns L/D To Reduce Fuel Burn," NASA ARMD Seedling Fund Phase I, February 25, 2014, http://nari.arc.nasa.gov/sites/default/files/SeedlingREYNOLDS.pdf

[23] Reynolds, K., Nguyen, N., Ting, E., and Urnes, J., "Wing Shaping Concepts Using Distributed Propulsion," Aircraft Engineering and Aerospace Technology: An International Journal, Vol. 86, No. 6, pp. 478-482, November 2014. DOI: 10.1108/AEAT-04-2014-0050

[24] Noll, T., Brown, J. M., Perez-Davis, M. E., Ishmael, S. D., and Gaier, M., "Investigation of the Helios Prototype Aircraft Mishap, Volume I Mishap Report," January 2004. https://www.nasa.gov/pdf/64317main_helios.pdf

[25] Dixon, S. L., *Thermodynamics of Turbomachinery*, Third Edition, Pergamon Press, Oxford, UK, 1978.

[26] Shapiro, A. H., *The Dynamics and Thermodynamics of Compressible Fluid Flow*, Vol. 1, Ronald Press, New York, 1953.

[27] Pratt & Whitney, "Pratt & Whitney's PW2000 Engine Family," https:// www.pw.utc.com/Content/Press_Kits/pdf/ce_pw2000_fact.pdf, 2013, Retrieval Date: September 12, 2017.

[28] Rolls-Royce, "Best Engine for the Airbus A330," https://www.rollsroyce. com/products-and-services/civil-aerospace/airlines/trent-700. aspx#/, 2015, Retrieval Date: September 12, 2017.

[29] Rolls-Royce, "1000 Times Better," https://www.rolls-royce.com/ products-and-services/civil-aerospace/airlines/trent-1000.aspx#/, 2017, Retrieval Date: September 12, 2017.

[30] Engine Alliance, "Introducing the GP7200," http://www.pw.utc.com/ Content/Press_Kits/pdf/ce_gp7200_fact.pdf, 2014, Retrieval Date: September 12, 2017.

[31] General ElectricAviation, "The GE90 Engine," https://www.geaviation. com/commercial/engines/ge90-engine, 2017, Retrieval Date: September 12, 2017.

[32] Nguyen, N., "Integrated Flight Dynamics Modeling of Flexible Aircraft with Inertial Force-Propulsion-Aeroelastic Coupling," 46th AIAA Aerospace Sciences Meeting and Exhibit, AIAA-2008-0194, January 2008. DOI: 10.2514/6.2008-194

[33] Nguyen, N., Ting, E., Nguyen, D., and Trinh, K., "Flutter Analysis of Mission-Adaptive Wing with Variable Camber Continuous Trailing Edge Flap," 55th AIAA/ASME/ASCE/AHS/ASC Structures, Structural Dynamics, and Materials Conference, AIAA-2014-0839, January 2014. DOI: 10.2514/6.2014-0839

[34] Nguyen, N. and Ting, E., "Inertial Force Coupling to Nonlinear Aeroelasticity of Flexible Wing Aircraft," AIAA Dynamics Specialists Conference, AIAA-2016-1094, January 2016. DOI: 10.2514/6.2016-1094

[35] Theodorsen, T., "General Theory of Aerodynamic Instability and the Mechanism of Flutter," NACA Rept. 496, Washington, D.C., 1949.

[36] Nguyen, N. and Hornby, G., "Trajectory Optimization Using Adjoint Method and Chebyshev Polynomial Approximation for Minimizing Fuel Consumption During Climb," AIAA Infotech@Aerospace Conference, AIAA-2013-5142, August 2013. DOI: 10.2514/6.2013-5142

[37] Burcham, F. W., Fullerton, C. G., Gilyard, G., Wolf, T., and Stewart, J., "A Preliminary Investigation of the Use of Throttles for Emergency Flight Control," AIAA 27th Joint Propulsion Conference, AIAA-91-2222, June 1999. DOI: 10.2514/6.1991-2222

[38] National Transportation Safety Board, "United Airlines Flight 232, McDonnell Douglas DC-10-10, Sioux Gateway Airport, Sioux City, Iowa, July 19, 1989," Aircraft Accident, Rept. PB90-910406, NTSB/ AAR-90/06, Washington, D.C., Nov. 1990.

[39] Csank, J., May, R. D., Litt, J. S., and Guo, T., "Control Design for a Generic Commercial Aircraft Engine," 46th AIAA Joint Propulsion Conference & Exhibit, AIAA-2010-6629, July, 2010, NASA/TM-2010-216811, October 2010. DOI: 10.2514/6.2010-6629

[40] Nguyen, N. and Stepanyan, V., "Flight-Propulsion Response Requirements for Directional Stability and Control," AIAA Infotech@Aerospace Conference, AIAA-2010-3471, April 2010. DOI: 10.2514/6.2010-3471